Latency-Aware Multi-Antenna SWIPT System With Battery-Constrained Receivers

Dileep Kumar, *Graduate Student Member, IEEE*, Onel L. Alcaraz López, *Member, IEEE*, Satya Krishna Joshi, *Member, IEEE*, and Antti Tölli, *Senior Member, IEEE*

Abstract—**Power splitting (PS) based simultaneous wireless information and power transfer (SWIPT) is considered in a multi-user multiple-input-single-output broadcast scenario. Specifically, we focus on jointly configuring the transmit beamforming vectors and receive PS ratios to minimize the total transmit energy of the base station under the user-specific latency and energy harvesting (EH) requirements. The battery depletion phenomenon is avoided by preemptively incorporating information regarding the receivers' battery state and EH fluctuations into the resource allocation design. The resulting time-average sum-power minimization problem is temporally correlated, non-convex (including mutually coupled latency-battery queue dynamics), and in general intractable. We use the Lyapunov optimization framework and derive a dynamic control algorithm to transform the original problem into a sequence of per-time-slot deterministic and independent subproblems. The latter are then solved via two alternative approaches: i) semidefinite relaxation combined with fractional programming, and ii) successive convex approximation. Furthermore, we design a low-complexity closed-form iterative algorithm exploiting the Karush-Kuhn-Tucker optimality conditions for a specific scenario with delay bounded batteryless receivers. Numerical results provide insights on the robustness of the proposed designs to realize an energy-efficient SWIPT system while ensuring latency and EH requirements in a time dynamic network.**

Index Terms—**Beamforming, battery dynamics, convex optimization, energy harvesting, Karush-Kuhn-Tucker conditions, Lyapunov framework, power splitting, queue backlogs, SWIPT, sum power minimization.**

I. INTRODUCTION

POWERING and supporting the seamless and autonomous operation of Internet-of-Things (IoT) deployments is becoming challenging given the exponential increase in the number of ubiquitous and low-power devices. On one hand, wired charging is usually cost-prohibitive and/or inconvenient to deploy anywhere, especially when considering industrial IoT deployments. On the other hand, traditional battery-powered solutions struggle with limited battery life and the corresponding replacement problem, which is neither economical nor eco-friendly. Unfortunately, the energy scavenging from environmental sources (e.g., solar, wind, thermal, etc) may be also inappropriate (at least as a standalone) for many use cases with stringent Quality-of-Service (QoS) requirements. This is because the associated energy supply is uncontrollable and can significantly oscillate according to temporal/geographical/environmental circumstances. Moreover, the ambient energy scavenging demand an add-on harvesting material and circuit, which in practice limits the form factor reduction to the desired levels for many use cases. As an appealing alternative, radio frequency (RF)-based wireless energy transfer (WET) allows efficient on-demand charging of low-power devices over the air, which simplifies servicing and maintenance, promotes form factor reduction and durability increase of the end devices, and thus contributes to the realization of scalable and sustainable wireless networks [3].

Wireless networks natively include wireless information transfer processes, hence WET appears naturally combined with them. The simultaneous wireless information and power transfer (SWIPT) technology, which enables efficient utilization of radio resources by wirelessly charging battery-limited devices while simultaneously conveying useful information [4], [5], [6], is an example of it. Specifically, the downlink multi-antenna broadcast SWIPT system has attracted much attention from the research community and has been widely studied in the literature. As an example, the early pioneering work [7] characterizes the underlying rate-energy trade-offs of a broadcast SWIPT system that includes a multi-antenna base-station (BS) communicating with several user equipments (UEs) in downlink. Therein, each UE may perform both energy harvesting (EH) and information decoding (ID) functions on the received signal, i.e., either by applying the time-switching (TS) [7] or power splitting (PS) [7], [8] protocol. Meanwhile, the authors in [9] investigate the problems of maximizing the effective capacity and energy efficiency by considering both PS and TS architectures subject to a fixed minimum harvested energy and fixed QoS delay requirements for receivers. Although a TS scheme simplifies the receiver design, it hinders the full exploitation of radio resources since

the wireless information and WET processes are not really simultaneous in time. Thus, motivating the use of PS schemes which generally achieve higher spectral efficiency [9], [10] and energy efficiency [9]. A comprehensive overview of the aforementioned PS and TS schemes and other less popular SWIPT schemes, such as the so-called spatial switching (SS) and integrated receiver (IR), is provided in [11].

It is worth highlighting that interference substantially reduces the data rate achievable at each link, thus it has an adverse impact on ID performance. Meanwhile, in terms of WET, the interference is not a foe but a friend since the power of interfering signals can easily be transformed into useful energy, and conceivably used for recharging EH UEs [12], [13], [14], [15]. Due to the simultaneous multi-user RF EH, the SWIPT beamformer design inherently has a multicast structure. Note that finding a good balance between EH and ID is key for an efficient SWIPT implementation. For scenarios with separated EH and ID receivers, the authors of [12] study the minimization of the worst-case mean square error (MSE) of the received information signals under transmit power and receive EH constraints. In [13], the transmit beamformer is designed to maximize the weighted sum of users' harvested power subject to per-user signal-to-interference-plus-noise ratio (SINR) requirements. Meanwhile, authors in [14] characterize the achievable rate-energy trade-off in a SWIPT multi-user MIMO interference channel. In [16], a joint beamforming and PS optimization is carried out to minimize the BS transmit power, under fixed SINR and EH QoS constraints per user, with the help of the semidefinite relaxation (SDR) framework. This work is extended in [17], wherein the authors develop a low-complexity and computationally efficient solution via second-order cone program (SOCP). Authors of [18] and [19] also extend [16] by studying and optimizing the transceiver design under MSE and EH constraints. Meanwhile, a joint transmit power allocation and receiver PS mechanism is proposed in [20] to maximize the minimum SINR at the UEs. Assuming co-located EH and ID receivers, the minimization of the sum power consumption is studied in [15], [21], and [22], while [23] considers the energy efficiency maximization, where beamforming vectors and PS ratios are jointly designed subject to a fixed minimum EH and SINR constraints per UE.

All the aforementioned works mainly focus on a downlink multi-user SWIPT system under fixed users' QoS requirements. Moreover, they assume that the instantaneous harvested energy is always sufficient to support the devices' computational and communication operations. However, the energy required to decode the received data increases with the downlink transmitted rate [24], [25], and thus the above assumption may not be always satisfied. Specifically, if the energy required for the information decoding operation surpasses the current energy availability, the UE could turn off, or at least interrupt the ID operations, thus causing a service outage. This critical problem has lately attracted significant research effort in diverse setups. For information-only transfer systems with limited energy availability at the receivers, authors of [24] investigate the downlink transmission strategies and provide the feasible maximum supported data rates, which are mainly restricted by the receivers' instantaneous battery levels. The previous work is extended to coordinated multi-cell systems in [25]. Meanwhile, authors of [26], [27], and [28] aim to maximize the network sum rate while considering the battery depletion problem, for which they establish a limited receiver battery constraint. In [26] and [28], the solutions are only based on the instantaneous states of the batteries, while [27] applies the Lyapunov optimization framework to design an online dynamic control algorithm.

The Lyapunov based solution has been widely used in many practical applications (as, e.g., in [29], [30], [31], and [32]) to transform the long-term average stochastic problem into a series of per-time-slot deterministic optimization subproblems, which do not require any a priori information on the system uncertainties, while efficiently capturing the non-stationary evolution of queue backlogs per user. In [29], the authors propose a SWIPT-enabled mechanism to increase the average secrecy throughput by considering the data and energy buffering at the wirelessly powered relays. Meanwhile, the authors of [30] design an online adaptive resource allocation policy to maximize the fairness among different mobile clients, while the trade-off between response delay and energy efficiency is studied in [31]. Finally, authors in [32] propose a task scheduling algorithm for SWIPT systems to minimize the energy consumption, while satisfying a minimum average data and task performing rate.

A. Contributions

Although the state-of-the-art research on SWIPT-enabled systems is vast, the increasingly stringent system QoS requirements, low energy availability, and battery dynamics over time still require extensive study, which motivates our research in this work. Specifically, we provide the joint optimization of transmit beamforming vectors and receive PS ratios that concurrently satisfies the user-specific latency and EH requirements of a PS-based SWIPT system. Our proposed radio resource allocation strategies preemptively incorporate information related to the users' battery state and EH fluctuations while efficiently avoiding the battery depletion phenomenon in a delay bounded time dynamic mobile access network. To the best of our knowledge, this paper, whose preliminary and reduced-length versions can be found in our earlier works [1], [2], is the first to jointly consider the interdependence of latency-battery dynamics for SWIPT-enabled systems. The key contributions of this paper are as follows:

- We formulate a long-term transmit energy minimization problem subject to users' probabilistic queue backlog constraint and a maximum harvested power requirement. The transmit beamforming vectors and receive PS ratios are jointly designed considering explicitly the minimum energy needed to decode downlink transmitted data messages and to support battery-limited receivers' operations. Our proposed radio resource allocation schemes allow meeting the latency and EH requirements at the UEs while avoiding their battery depletion.
- We employ the Lyapunov optimization framework, specifically the drift-plus-penalty function, to transform

the time-average problem into a sequence of per-time-slot deterministic subproblems, while efficiently capturing the non-stationary evolution of queue backlogs. To circumvent the temporally correlated user-specific battery and EH constraints, we introduce a virtual spare battery queue for each user. A dynamic control algorithm is then provided for solving the time-correlated and cumbersome average sum-power minimization problem.

- The beamformers and PS ratios are coupled in SINR and EH expressions, and are not jointly convex. To circumvent this, two alternative approaches, namely SDR combined with fractional programming (FP) quadratic transform technique, and a linear Taylor series approximation via successive convex approximation (SCA) framework, are adopted. Both proposed methods achieve efficient solutions, each with specific convergence and complexity characteristics. Specifically, the SDR-FP based method provides faster convergence in terms of the required approximation point updates for the considered setup configuration. In contrast, the SCA framework has much lower computational complexity per iteration, and the optimized beamformers are obtained directly. It is worth highlighting that the constrained optimization schemes proposed in [16], [17], [18], [19], [20], [21], [22], and [23] can not be used directly here due to the underlying interdependence of latency-battery queue dynamics. Thus, our proposed solutions are significantly more advanced, and provide a systematic approach for solving problems with mutually coupled and non-linear time-varying constraints.

- A low-complexity and computationally efficient iterative algorithm is proposed for a special scenario where the latency constrained SWIPT-enabled receivers operate without energy storage, and the harvested energy is made immediately available to support their operations [16], [17]. Specifically, the proposed algorithm exploits the Karush-Kuhn-Tucker (KKT) optimality conditions, and requires evaluating only closed-form mathematical expressions. This leads to computationally efficient, thus, latency-friendly, implementations.

The proposed methods provide insights into the trade-offs between the long-term achievable harvested energy at UEs and required transmit energy at the BS, while ensuring the user-specific latency and minimum battery energy requirements to support the persistent receivers' operations. The simulation results manifest the robustness of the proposed designs to realize energy-efficient SWIPT systems for delay bounded applications in a time dynamic mobile access network.

B. Organization and Notations

The remainder of this paper is organized as follows. In Section II, we describe the system architecture and optimization problem. Section III provides a dynamic control algorithm for the average sum-power minimization problem. In Section IV, we propose the joint beamforming and PS optimization. In Section V, we study the batteryless scenario. Simulation results are presented in Section VI, while conclusions are drawn in Section VII.

Notations: We use italic, boldface lower- and upper-case letters to denote scalars, vectors and matrices, respectively. Notation $\mathbb{C}^{N \times M}$ represents the space of $N \times M$ complex matrices. The norm and the real part of a complex number is represented with $|\cdot|$ and $\Re\{\cdot\}$, respectively. For an arbitrary-size matrix $\mathbf{X}$, the superscript $\mathbf{X}^{-1}$, $\mathbf{X}^{\mathrm{H}}$ and $\mathbf{X}^{\mathrm{T}}$ donates respectively inverse, conjugate transpose and transpose operation. $[\mathbf{X}]_{m,n}$ is the (m, n)-th element of $\mathbf{X}$, and $[x]^+ \triangleq \max(0, x)$. Notation $\mathbb{E}[\cdot]$ represents the statistical expectation operation.

II. System Architecture and Problem Formulation

A. System Model

We consider a multi-user multiple-input single-output (MU-MISO) SWIPT system as shown in Fig. 1. Here, a set $\mathcal{K} \triangleq \{1, 2, \ldots, K\}$ of single antenna UEs is served by a BS equipped with N_t transmit antennas in the downlink. For simplicity, but without loss of generality, we consider a time-slotted frame structure where the slots are normalized to an integer value, i.e., $t \in \{T_f, 2T_f, \ldots\}$ with a duration of T_f seconds each. Let $\mathbf{h}_k(t), \mathbf{f}_k(t) \in \mathbb{C}^{N_t \times 1}$ denote respectively the downlink channel vector and transmit beamforming vector corresponding to the k-th UE during time slot t. Then, the signal received at the k-th UE can be expressed as

$$y_k(t) = \mathbf{h}_k^{\mathrm{H}}(t)\mathbf{f}_k(t)d_k(t)$$
$$+ \sum_{u \in \mathcal{K} \setminus k} \mathbf{h}_k^{\mathrm{H}}(t)\mathbf{f}_u(t)d_u(t) + w_k(t), \quad (1)$$

where $w_k \in \mathcal{CN}(0, \sigma_k^2)$ denotes the additive white Gaussian noise (AWGN) at the receiver, and d_k is the downlink transmitted data symbol. Moreover, we assume independent and normalized data symbols, i.e., $\mathbb{E}\{d_k d_u^*\} = 0$ and $\mathbb{E}\{|d_k|^2\} = 1$, $\forall k, u \in \mathcal{K}$ and $k \neq u$.

Similar to [7], [8], [15], [16], [17], [18], [19], [20], [21], [22], and [23], we assume that each UE $k \in \mathcal{K}$ implements PS on the received signal $y_k(t)$ for simultaneous ID and EH as shown in Fig. 1. Let $\rho_k(t) \in [0, 1]$ represent the PS ratio to the ID circuit of k-th UE during time slot t. Then, the portion of the signal split to the ID circuit can be expressed as

$$y_k^{\mathrm{ID}}(t) = \sqrt{\rho_k(t)}\Big(\mathbf{h}_k^{\mathrm{H}}(t)\mathbf{f}_k(t)d_k(t)$$
$$+ \sum_{u \in \mathcal{K} \setminus k} \mathbf{h}_k^{\mathrm{H}}(t)\mathbf{f}_u(t)d_u(t) + w_k(t)\Big) + \tilde{z}_k(t), \quad (2)$$

where $\tilde{z}_k \in \mathcal{CN}(0, \delta_k^2)$ is the additive noise at the ID circuit of k-th UE. The received SINR of k-th UE is given by

$$\Gamma_k(t) = \frac{\rho_k(t)|\mathbf{h}_k^{\mathrm{H}}(t)\mathbf{f}_k(t)|^2}{\rho_k(t)\sum\limits_{u \in \mathcal{K} \setminus k}|\mathbf{h}_k^{\mathrm{H}}(t)\mathbf{f}_u(t)|^2 + \rho_k(t)\sigma_k^2 + \delta_k^2}. \quad (3)$$

Meanwhile, the remaining portion of the signal split to the EH circuit of k-th UE during time slot t is given by

$$y_k^{\mathrm{EH}}(t) = \sqrt{1 - \rho_k(t)}\Big(\mathbf{h}_k^{\mathrm{H}}(t)\mathbf{f}_k(t)d_k(t)$$
$$+ \sum_{u \in \mathcal{K} \setminus k} \mathbf{h}_k^{\mathrm{H}}(t)\mathbf{f}_u(t)d_u(t) + w_k(t)\Big). \quad (4)$$
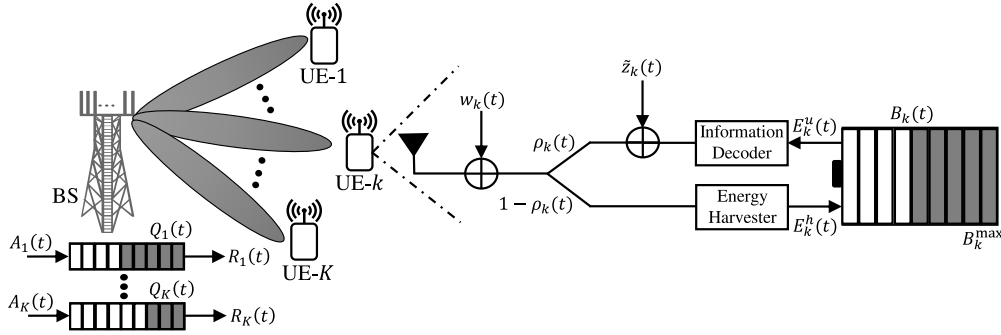
Fig. 1. The SWIPT system consists of one BS with user-specific queues, and multiple battery-limited UEs, where each UE implements the PS scheme to perform EH and ID simultaneously.

Then, the harvested power at the EH circuit of k-th UE is given by

$$E_k^h(t) = \zeta_k \big(1 - \rho_k(t)\big) \Big(\sum_{j \in \mathcal{K}} |\mathbf{h}_k^H(t)\mathbf{f}_j(t)|^2 + \sigma_k^2 \Big), \quad (5)$$

where $\zeta_k \in [0, 1)$ represents the energy conversion efficiency.

Note that we consider an EH model, as in [7], [8], [16], and [17], where the output direct current (DC) increases linearly with the input RF power level. However, in practice, the energy conversion efficiency of a practical EH circuit is not constant due to the non-linearities introduced by, e.g., resistance, capacitance, and diode-connected transistors [33]. Note that there is no generic EH model which can capture all practical issues of EH circuit components [34]. Therefore, we are considering a broadly recognized, yet simple, linear model for analytical tractability and to facilitate the discussion. Indeed, we aim to capture, for the first time, the underlying interdependence of latency-battery queue dynamics for SWIPT-enabled time dynamic systems, for which leveraging a simple EH model is a natural first step. Moreover, the results and the performance trends shown in this paper should still, approximately, hold for the moderate input power level regime [32, Fig. 4]. Considering a more involved EH model, which efficiently accounts for the sensitivity and saturation impairments of the non-linear circuit components, is an interesting topic for future extensions of this work.

B. Queueing & Latency Model at Network

We assume that the BS has queue buffers to store the network layer data of UEs [35, Ch. 5]. Let $Q_k(t)$ denote the queue backlog of k-th UE during time slot t, which evolves as

$$Q_k(t + 1) = \big[Q_k(t) - R_k(t) + A_k(t) \big]^+, \quad \forall k, \quad (6)$$

where $[x]^+ \triangleq \max(x, 0)$, $R_k(t) \triangleq \log_2(1 + \gamma_k(t))$ is the downlink rate, and $\gamma_k(t)$ denotes the achievable SINR of k-th UE during time slot t. In (6), $A_k(t)$ denotes the downlink data arrival with a mean arrival rate of $\mathbb{E}[A_k(t)] = \alpha_k, \forall k \in \mathcal{K}$.

According to Little's law, the average delay (or latency) is proportional to long-term time-average queue length as $\lim_{T \to \infty} \frac{1}{T} \sum_{t=0}^{T-1} \mathbb{E}[Q_k(t)]$ [36, Ch. 1.4]. Thus, we can use the queue backlogs $\{Q_k(t)\}$ as users' latency measures, and impose the allowable threshold $\{Q_k^{\text{th}}\}$ to each time slot.
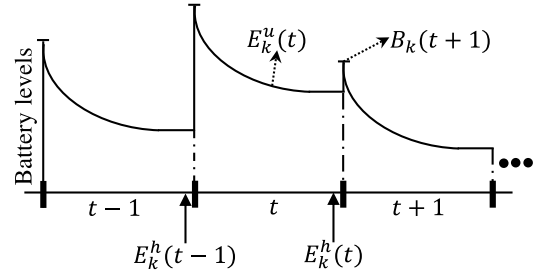

Fig. 2. An illustration of the receivers' battery storage and consumption model at the k-th UE.

Specifically, we consider a probabilistic constraint on user-specific queue length [37], defined as

$$\Pr\big\{ Q_k(t) \geq Q_k^{\text{th}} \big\} \leq \epsilon, \quad \forall t, \quad (7)$$

where ϵ is a tolerable probability for delay bound violation.

C. Battery Storage & Consumption Model at Receiver

The k-th UE is equipped with a battery of finite capacity B_k^{max}. The battery energy level decreases in accordance with the circuit power consumption and the decoding operations of the downlink received data [24], [25], [26], [27], [28]. The EH circuit allows the UEs to recharge their battery by collecting the required energy from received RF signals (see (5)). Similar to [26] and [27], we assume that the EH system adopts the *harvest-store-use* strategy [4, Sec. III], wherein the harvested energy in a given time slot can be only available in the subsequent time slots, as shown in Fig. 2. Thus, the battery dynamics $B_k(t + 1)$ of the k-th UE at the beginning of the time slot $(t + 1)$ is given by

$$B_k(t+1) = \min\Big\{ B_k^{\text{max}}, \ \big[B_k(t) - E_k^u(t) \big]^+ + E_k^h(t) \Big\}, \quad \forall k, \quad (8)$$

where $E_k^h(t)$ is the harvested energy defined in (5). Moreover, $E_k^u(t)$ represents the energy spent by the k-th UE during time slot t, which we model as

$$E_k^u(t) = T_f\big(P_k^{\text{cir}} + P_k^{\text{dec}}(t) \big), \quad \forall k, \quad (9)$$

where P_k^{cir} is the fixed power consumed by the receiver, including the front-end circuit, and reporting power consumption of the UE to the BS. In (9), $P_k^{\text{dec}}(t)$ is the power consumed by the decoding process. Note that the overall energy to be consumed in each time slot must not exceed the energy currently available in the users' battery, i.e., $0 \leq E_k^u(t) \leq B_k(t)$, $\forall t, k$. Specifically, by incorporating the receivers' battery state information in the design of beamformers and PS ratios, the BS can adequately allocate the required resources to ensure, i.e., maximum supported rates $R_k^{\max}(t)$ and maximum required EH $E_k^{\max}(t)$ for each user at each time slot.

The circuit power P_k^{cir} is assumed to be a constant for each user. On the other hand, $P_k^{\text{dec}}(t)$ mainly depends on the transmitted data rates, defined as $P_k^{\text{dec}}(t) \triangleq f(R_k(t))$, $\forall k \in \mathcal{K}$. It is worth highlighting that there is no standardized and extensively recognized model for $f(R_k(t))$ in the research community. However, there is a consensus about the fact that the decoding consumption always increases with the downlink transmit rate. Herein, we adopt the model presented in [24], which states that the energy consumed is linearly increasing with the downlink transmitted data rates. Specifically, $f(R_k(t)) \triangleq \vartheta_k^d R_k(t)$ where $\vartheta_k^d > 0$ reflects the energy efficiency [Joules/bit] of the decoder implementation at the receiver device. Thus, combined with $P_k^{\text{dec}}(t)$ and expression (9), the maximum allowable downlink rates $R_k^{\max}(t)$ of each user k can be expressed as[1] [24, Sec. II]

$$R_k(t) \leq R_k^{\max}(t) \triangleq \frac{1}{\vartheta_k^d}\left(\frac{E_k^u(t) - T_f P_k^{\text{cir}}}{T_f}\right), \quad \forall k. \quad (10)$$

Note that due to the stochastic nature of the radio channel, there exists a non-negligible probability that the links between the BS and certain UEs are in poor conditions (i.e., in a deep fading state). Thus, scheduling such UEs will probably provide little (if any) benefit. However, storing the energy and waiting for better channel gains may improve the network performance. Therefore, at the beginning of each time slot, the resource allocation process at the BS should take into account the user-specific battery charge levels, and accordingly assign the downlink rates. From (9), we can observe that even if the k-th UE is not served at a given scheduling time slot t, its battery will still decrease according to $T_f P_k^{\text{cir}}$. This fixed energy consumption impacts the resource allocation algorithm for the EH process, i.e., the battery energy should not be instantaneously depleted and there should be always sufficient energy stored in the receiver's battery to support its persistent operations at each time slot.

The battery storage capacity of the k-th UE is limited by $B_k^{\max}$, and the overflow (or extra) harvested energy will be eventually discarded by the user device. Thus, the harvested energy at each time slot t can be upper bounded by

$$E_k^h(t) \leq E_k^{\max}(t) \triangleq B_k^{\max} - B_k(t), \quad \forall k. \quad (11)$$

To summarize, the current battery charge level at each UE strictly constrains both the maximum supported downlink

[1]Note that the beamformer design and PS strategy proposed in the paper can be extended by adopting the appropriate maximum supported rate (10) corresponding to any specific implementation of the decoding power consumption model [24, Sec. II].

transmit rates (10) and the maximum EH requirements (11) at each time slot. We assume a standard time division duplex (TDD)-based channel state information (CSI) acquisition from reciprocal uplink, where the current battery energy availability is also reported by the UEs [24], [25], [26], [27], [28]. Hence, the resource allocation process not only considers CSI, but also the residual energy in the receivers' battery, for the joint design of transmit beamforming vectors and receive PS ratios in a delay bounded time dynamic mobile access network.

D. Problem Formulation

Our objective is to design a power-efficient resource allocation scheme that satisfies the latency requirement of each user while taking into account the user-specific battery energy limitations. Specifically, we jointly optimize transmit beamforming vectors and receive PS ratios in order to minimize the BS average transmit power subject to a probabilistic queue backlog constraint and a maximum harvested power requirement per user. Furthermore, the resource allocation strategies are designed by preemptively incorporating the receivers' battery and EH fluctuations while efficiently avoiding the battery depletion phenomenon. The network average transmit sum-power minimization problem can be formulated as

$$\min_{\{\mathbf{f}_k(t), \rho_k(t)\}, \, \forall t} \, \lim_{T \to \infty} \frac{1}{T} \sum_{t=0}^{T-1} \sum_{k \in \mathcal{K}} \mathbb{E}\big[\|\mathbf{f}_k(t)\|^2\big] \quad (12a)$$

$$\text{s.t. } \Pr\big\{Q_k(t) \geq Q_k^{\text{th}}\big\} \leq \epsilon, \quad \forall k, \, \forall t, \quad (12b)$$

$$R_k(t) \leq R_k^{\max}(t), \quad \forall k, \, \forall t, \quad (12c)$$

$$E_k^h(t) \leq E_k^{\max}(t), \quad \forall k, \, \forall t, \quad (12d)$$

$$0 \leq \rho_k(t) \leq 1, \quad \forall k, \, \forall t, \quad (12e)$$

where the expectation operation in (12a) is with respect to random channel states and data arrivals processes. Note that (12b) guarantees that the queue backlog of k-th UE at each time slot t is less than Q_k^{th} with probability $1 - \epsilon$, thus, it ensures the desired users' latency requirements.

III. DYNAMIC CONTROL ALGORITHM VIA LYAPUNOV FRAMEWORK

Problem (12) consists of a time-average sum-power objective function (12a), a non-linear probabilistic constraint (12b), rate constraints (12c) including coupled and non-convex SINR expressions, EH constraint (12d) including time-correlated battery energy dynamics, which cannot be addressed directly in a tractable manner. In this section, we first handle the time-average and probabilistic intractability, and then provide an online dynamic control algorithm exploiting the drift-plus-penalty framework and the Lyapunov optimization theory [35]. The proposed convex relaxations for the coupled and non-convex constraints are later provided in Section IV.

We start by applying the well-known Markov's inequality [36], and transform the non-linear probabilistic queue-length constraint (12b) as

$$\Pr\big\{Q_k(t) \geq Q_k^{\text{th}}\big\} \leq \mathbb{E}[Q_k(t)]/Q_k^{\text{th}} \leq \epsilon, \quad \forall k \in \mathcal{K}.$$

Thereby, problem (12) can be equivalently rewritten as

$$\min_{\{\mathbf{f}_k(t),\rho_k(t)\},\,\forall t} \lim_{T\to\infty} \frac{1}{T} \sum_{t=0}^{T-1} \sum_{k\in\mathcal{K}} \mathbb{E}\big[\|\mathbf{f}_k(t)\|^2\big] \quad (13a)$$

$$\text{s.t.} \lim_{T\to\infty} \frac{1}{T} \sum_{t=0}^{T-1} \mathbb{E}\big[Q_k(t)\big] \leq \epsilon Q_k^{\text{th}}, \quad \forall k,$$

$$\text{constraints } (12c)-(12e). \quad (13b)$$

Next, the time-average constraint (13b) is tackled by recasting it as a queue stability problem [35, Ch.5]. Specifically, we define a virtual data queue $Z_k(t)$ for each user k, which evolves as

$$Z_k(t+1) = \big[Z_k(t) + Q_k(t+1) - \epsilon Q_k^{\text{th}}\big]^+, \quad \forall k. \quad (14)$$

Note that the inequality constraint (13b) is ensured only if the associated virtual queues $\{Z_k(t)\}_{\forall k}$ are stabilized [35, Theorem 2.5]. Thus, to stabilize the virtual queues in (14), we employ the Lyapunov optimization framework, and design a dynamic control algorithm with long-term stability requirements. It is worth highlighting that the feasible control action sets are coupled over time due to the temporally correlated user-specific battery charge level (12d) [26], [27]. To circumvent this issue, we introduce a virtual battery queue $U_k(t)$ for each user k, defined as

$$U_k(t) \triangleq B_k^{\max} - B_k(t), \quad \forall k. \quad (15)$$

From (15), we can observe that the spare energy availability at the receivers' battery increases inversely with the value of $U_k(t)$, $\forall k \in \mathcal{K}$. Thus, to jointly stabilize the coupled virtual data queues (14) and battery queues (15), we now define a weighted quadratic Lyapunov function [35]

$$\mathcal{L}(\mathbf{\Psi}(t)) \triangleq \frac{1}{2} \sum_{k\in\mathcal{K}} \big\{Z_k(t)^2 + \omega_k U_k(t)^2\big\}, \quad (16)$$

where $\mathbf{\Psi}(t) = \big[Z_k(t), Q_k(t), U_k(t), B_k(t)\big| \forall k \in \mathcal{K}\big]$ and $\omega_k > 0$ is a linear scaling factor on the spare battery capacity of the k-th UE. Note that the parameter $\{\omega_k\}_{\forall k}$ in (16) can be considered as a free parameter (e.g., it may reflect energy to data bits conversion factor), which balances the user-specific contributions of latency-battery queue in the Lyapunov function. Specifically, different scaling on the virtual battery queue might lead to a different Pareto optimal allocation of resources.[2] Then, the Lyapunov drift between two consecutive time slot is given by

$$\triangle(\mathbf{\Psi}(t)) = \frac{1}{2}\mathbb{E}\big[\mathcal{L}(\mathbf{\Psi}(t+1)) - \mathcal{L}(\mathbf{\Psi}(t))\big|\mathbf{\Psi}(t)\big] \quad (17a)$$

$$= \frac{1}{2}\mathbb{E}\bigg[\sum_{k\in\mathcal{K}}\Big\{\big(Z_k(t+1)^2 - Z_k(t)^2\big)$$

$$+ \omega_k\big(U_k(t+1)^2 - U_k(t)^2\big)\Big\}\bigg|\mathbf{\Psi}(t)\bigg]. \quad (17b)$$

---

[2]The user-specific priority weights $\{\omega_k\}_{\forall k}$ corresponding to the spare battery capacity (16) are design parameters that can be tuned based on available statistical information, e.g., latency-battery queue states and channel conditions, to achieve the desired trade-off between BS transmit energy and receiver battery charge level. In fact, this is an interesting topic for future extensions.

Next, by using expressions (6), (8), (14) and (15) in (17), and after some algebraic simplifications, an upper bound for the Lyapunov drift $\triangle(\mathbf{\Psi}(t))$ is obtained as

$$\triangle(\mathbf{\Psi}(t)) \leq \Omega - \mathbb{E}\bigg[\sum_{k\in\mathcal{K}}\big(Q_k(t) + A_k(t) + Z_k(t)\big)R_k(t)\big|\mathbf{\Psi}(t)\bigg]$$

$$- \mathbb{E}\bigg[\sum_{k\in\mathcal{K}}\omega_k\big(B_k^{\max} - B_k(t)\big)E_k^h(t)\big|\mathbf{\Psi}(t)\bigg], \quad (18)$$

where Ω is a positive constant term. More specifically, $\Omega = \zeta_Q + \Phi_Q(t) + \zeta_B + \Phi_B(t)$, while the following conditions[3] are satisfied in all time slots [35]:

$$\zeta_Q \geq \frac{1}{2}\mathbb{E}\bigg[\sum_{k\in\mathcal{K}}\big\{A_k(t)^2 + R_k(t)^2\big\}\big|\mathbf{\Psi}(t)\bigg], \quad (19a)$$

$$\Phi_Q(t) = \sum_{k\in\mathcal{K}}\bigg\{\frac{1}{2}(\epsilon Q_k^{\text{th}})^2 + \frac{1}{2}Q_k(t)^2 + Z_k(t)Q_k(t)$$

$$+ \big(Q_k(t) + Z_k(t)\big)A_k(t)\bigg\}, \quad (19b)$$

$$\zeta_B \geq \frac{1}{2}\mathbb{E}\bigg[\sum_{k\in\mathcal{K}}\big\{\omega_k E_k^u(t)^2 + \omega_k E_k^h(t)^2\big\}\big|\mathbf{\Psi}(t)\bigg], \quad (19c)$$

$$\Phi_B(t) = \sum_{k\in\mathcal{K}}\omega_k\big(B_k^{\max} - B_k(t)\big)E_k^u(t). \quad (19d)$$

We define the drift-plus-penalty function [35] for (13) as

$$\triangle(\mathbf{\Psi}(t)) + V\mathbb{E}\bigg[\sum_{k\in\mathcal{K}}\|\mathbf{f}_k(t)\|^2\big|\mathbf{\Psi}(t)\bigg], \quad (20)$$

where $V \geq 0$ is a trade-off parameter. Thus, by minimizing the upper bound of (20) subject to constraints (12c) - (12e) at each time slot, we can ensure the user-specific latency requirements and maintain the required battery energy levels at the receiver, while minimizing the sum-power objective function (12a). Herein, we employ the concept of opportunistic minimization of an expectation [35, Ch. 1.8] to minimize the upper bound of (20), and obtain a series of per-time-slot deterministic problem. Moreover, each subproblem (21) can be independently solved based on the current queue buffer, battery charge level, and CSI, as summarized in Algorithm 1.

Note that we have conveniently introduced the non-negative auxiliary variables $\{\gamma_k(t), e_k(t)\}_{\forall k}$ to ease the problem tractability. Nevertheless, this does not affect the corresponding solution since constraints (21b) and (21c) hold with equality at the optimality [38]. Moreover, for a given queue state at beginning of each time slot t, the transmit beamformers and receive PS ratios can be computed independently as described in Section IV.

IV. JOINT BEAMFORMERS AND PS RATIOS DESIGN

The joint beamformers and PS ratios design problem (21) introduced in Algorithm 1 is still intractable due to the non-convex SINR expressions (21b), and the coupling between the optimization variables $\{\mathbf{f}_k(t), \rho_k(t), \gamma_k(t)\}$ in (21b) and the optimization variables $\{\mathbf{f}_k(t), \rho_k(t), e_k(t)\}$ in (21c). In this

---

[3]To obtain (18), we used $([a_1 + a_2 - a_3]^+)^2 \leq (a_1 + a_2 - a_3)^2$, $\forall\{a_1, a_2, a_3\} \geq 0$. Further, we have assumed that the second moments of data arrival $\mathbb{E}[A_k(t)^2|\mathbf{\Psi}(t)]$ and transmission $\mathbb{E}[R_k(t)^2|\mathbf{\Psi}(t)]$ processes in (19a), and energy utilized $\mathbb{E}[E_k^u(t)^2|\mathbf{\Psi}(t)]$ and harvested $\mathbb{E}[E_k^h(t)^2|\mathbf{\Psi}(t)]$ processes in (19c) for all $k \in \mathcal{K}$ are bounded [35, Ch. 5].

Algorithm 1 Dynamic Control Algorithm for (12)

1 For a given time slot t, obtain battery levels $\{B_k(t)\}$ and compute $R_k^{\max}(t)$ using (10)

2 Observe the current queue backlogs $\{Q_k(t), Z_k(t)\}$, and solve the following problem:

$$\min_{\substack{\{\mathbf{f}_k(t), \gamma_k(t), \\ e_k(t), \rho_k(t)\}}} V \sum_{k \in \mathcal{K}} \|\mathbf{f}_k(t)\|^2 - \sum_{k \in \mathcal{K}} \omega_k \left(B_k^{\max} - B_k(t)\right) e_k(t)$$

$$- \sum_{k \in \mathcal{K}} \left(Q_k(t) + A_k(t) + Z_k(t)\right) \log_2(1 + \gamma_k(t)) \quad (21\text{a})$$

$$\text{s.t. } \gamma_k(t) \leq \frac{\rho_k(t)|\mathbf{h}_k^{\mathrm{H}}(t)\mathbf{f}_k(t)|^2}{\rho_k(t) \sum_{u \in \mathcal{K} \setminus k} |\mathbf{h}_k^{\mathrm{H}}(t)\mathbf{f}_u(t)|^2 + \rho_k(t)\sigma_k^2 + \delta_k^2}, \quad \forall k, \quad (21\text{b})$$

$$e_k(t) \leq \zeta_k \left(1 - \rho_k(t)\right) \left(\sum_{j=1}^{K} |\mathbf{h}_k^{\mathrm{H}}(t)\mathbf{f}_j(t)|^2 + \sigma_k^2\right), \quad \forall k, \quad (21\text{c})$$

$$\log_2(1 + \gamma_k(t)) \leq R_k^{\max}(t), \quad \forall k, \quad (21\text{d})$$

$$e_k(t) \leq E_k^{\max}(t), \quad \forall k, \quad (21\text{e})$$

3 $\qquad\qquad 0 \leq \rho_k(t) \leq 1, \quad \forall k. \quad (21\text{f})$

4 Update queues $\{Q_k(t+1)\}$ and $\{Z_k(t+1)\}$ by using (6) and (14), respectively

5 Update battery levels $\{B_k(t+1)\}$ by using (8)

6 Set $t = t+1$, and go to step 1

---

section, the coupled and non-convex constraints in (21) are handled by using two alternative approaches: i) SDR combined with recently proposed FP quadratic transform technique [39], and ii) linear Taylor series approximation via SCA framework [40]. Both proposed methods achieve efficient solutions, each with specific convergence and complexity characteristics. Specifically, for the considered setup configurations, the SDR-FP based method provides faster convergence in terms of the required approximation point updates. In contrast, the SCA framework has considerably lower computational complexity per iteration and the optimized beamforming vectors are obtained directly, which will become clear in the following.

It is worth highlighting that due to the underlying inter-dependence of latency-battery queue dynamics, the constrained optimization schemes described in [16], [17], [18], [19], [20], [21], [22], and [23] can not be used directly to solve (21). Thus, our proposed solutions are significantly more advanced, and provide a systematic approach for handling problems with mutually coupled constraints. Further, proposed approaches provide valuable insights on the joint optimization of beamformers and PS ratios that concurrently satisfies the latency and EH requirements per user, which is inherently an intractable and NP-hard optimization problem. Note that in both approaches, the non-convex problem (21) is first recast as a sequence of convex subproblems, and then iteratively solved until the desired convergence of the objective function (21a). In the following, we omit the time index t to simplify the notation.

A. Solution of (21) via SDR-FP Framework

To begin with, let us define $\mathbf{F}_k \triangleq \mathbf{f}_k \mathbf{f}_k^{\mathrm{H}}, \ \forall k \in \mathcal{K}$. The main idea behind the SDR framework is to drop the

rank-one constraints, e.g., replace each semidefinite rank-one matrix $\mathbf{F}_k$ by a general-rank positive semidefinite matrix, i.e., $\mathbf{F}_k \succeq 0, \ \forall k \in \mathcal{K}$. Then, an additional post-approximation procedure is required to obtain rank-one beamforming vectors using, e.g., eigen-decomposition and possibly combined with some randomization techniques [41], [42], as will become clear in the following. Thus, by applying the standard SDR technique to (21), and after some algebraic simplifications, we obtain the following relaxed problem

$$\min_{\substack{\{\mathbf{F}_k, \gamma_k, \\ e_k, \rho_k\}}} V \sum_{k \in \mathcal{K}} \mathrm{Tr}(\mathbf{F}_k) - \sum_{k \in \mathcal{K}} \omega_k (B_k^{\max} - B_k) e_k$$

$$- \sum_{k \in \mathcal{K}} (Q_k + A_k + Z_k) \log_2(1 + \gamma_k) \quad (22\text{a})$$

$$\text{s.t. } \frac{1}{\gamma_k} \mathbf{h}_k^{\mathrm{H}} \mathbf{F}_k \mathbf{h}_k - \sum_{u \in \mathcal{K} \setminus k} \mathbf{h}_k^{\mathrm{H}} \mathbf{F}_u \mathbf{h}_k \geq \sigma_k^2 + \frac{\delta_k^2}{\rho_k}, \quad \forall k, \quad (22\text{b})$$

$$\frac{1}{e_k} \left(\sum_{j=1}^{K} \mathbf{h}_k^{\mathrm{H}} \mathbf{F}_j \mathbf{h}_k + \sigma_k^2\right) \geq \frac{1}{\zeta_k(1 - \rho_k)}, \quad \forall k, \quad (22\text{c})$$

$$\gamma_k \leq 2^{R_k^{\max}} - 1, \quad \forall k, \quad (22\text{d})$$

$$e_k \leq E_k^{\max}, \quad \forall k, \quad (22\text{e})$$

$$0 \leq \rho_k \leq 1, \quad \forall k, \quad (22\text{f})$$

$$\mathbf{F}_k \succeq 0, \quad \forall k, \quad (22\text{g})$$

where $\mathrm{Tr}(\cdot)$ denotes the trace operation. Note that the reformulated problem (22) is still non-convex due to the coupling between variables $\{\mathbf{F}_k, \gamma_k\}$ in (22b) and $\{\mathbf{F}_k, e_k\}$ in (22c). Thus, managing the mutually coupled EH and SINR combinations is considerably more challenging than conventional constrained optimization with a fixed QoS requirement per user [16], [17]. To handle the fractional non-convexity in (22), we use the recently proposed FP quadratic transform technique [39], also reproduced in Proposition 1, that has been shown to converge to a local solution. Specifically, the FP quadratic transform techniques decouple the numerator and the denominator of the concave-convex functions, thereby enabling the iterative optimization between primal and auxiliary variables. This strategy works well for a variety of optimization problems, including scheduling, power control, and beamformer design [39].

Proposition 1: Given a non-negative function $A(\mathbf{x}) \geq 0$, a strictly positive function $B(\mathbf{x}) > 0$, and a monotonic function $f(\cdot) : \mathbb{R} \mapsto \mathbb{R}$, the coupled fractional constraint $f\left(\frac{A(\mathbf{x})}{B(\mathbf{x})}\right)$ is equivalent to $f\left(2\varpi\sqrt{A(\mathbf{x})} - \varpi_k^2 B(\mathbf{x})\right)$, when the auxiliary variable ϖ has the optimal value $\varpi^{(\star)} = \frac{\sqrt{A(\mathbf{x})}}{B(\mathbf{x})}$.

Proof: Proposition 1 can be easily proved by following the steps in [39, Section II]. $\qquad \square$

1) Convex Approximation for Constraint (22b): By using Proposition 1, the fractional term in (22b)

$$\frac{1}{\gamma_k} \mathbf{h}_k^{\mathrm{H}} \mathbf{F}_k \mathbf{h}_k, \quad \forall k, \quad (23\text{a})$$

is equivalent to

$$2\nu_k \sqrt{\mathbf{h}_k^{\mathrm{H}} \mathbf{F}_k \mathbf{h}_k} - \nu_k^2 \gamma_k, \quad \forall k, \quad (23\text{b})$$

when the auxiliary variable ν_k has the optimal value

$$\nu_k^{(\star)} = \frac{1}{\gamma_k}\sqrt{\mathbf{h}_k^{\mathrm{H}}\mathbf{F}_k\mathbf{h}_k}, \quad \forall k. \tag{23c}$$

2) Convex Approximation for Constraint (22c)*:* Similarly, by using Proposition 1, the fractional term in (22c)

$$\frac{1}{e_k}\Big(\sum_{j=1}^{K}\mathbf{h}_k^{\mathrm{H}}\mathbf{F}_j\mathbf{h}_k + \sigma_k^2\Big), \quad \forall k, \tag{24a}$$

is equivalent to

$$2\mu_k\sqrt{\sum_{j=1}^{K}\mathbf{h}_k^{\mathrm{H}}\mathbf{F}_j\mathbf{h}_k + \sigma_k^2} - \mu_k^2 e_k, \quad \forall k, \tag{24b}$$

when the associated auxiliary variable μ_k has the optimal value

$$\mu_k^{(\star)} = \frac{1}{e_k}\sqrt{\sum_{j=1}^{K}\mathbf{h}_k^{\mathrm{H}}\mathbf{F}_j\mathbf{h}_k + \sigma_k^2}, \quad \forall k. \tag{24c}$$

3) Approximated Convex Subproblem: By setting a fixed approximation point $\{\nu_k^{(i)}, \mu_k^{(i)}\}$, and substituting (23b) and (24b) into (22b) and (22c), respectively, the problem (22) can be expressed in convex form as

$$\min_{\substack{\{\mathbf{F}_k, \gamma_k, \\ e_k, \rho_k\}}} V\sum_{k\in\mathcal{K}}\mathrm{Tr}(\mathbf{F}_k) - \sum_{k\in\mathcal{K}}\omega_k(B_k^{\max} - B_k)e_k$$
$$- \sum_{k\in\mathcal{K}}(Q_k + A_k + Z_k)\log_2(1 + \gamma_k) \tag{25a}$$

$$\text{s.t. } 2\nu_k^{(i)}\sqrt{\mathbf{h}_k^{\mathrm{H}}\mathbf{F}_k\mathbf{h}_k} - \big(\nu_k^{(i)}\big)^2\gamma_k$$
$$- \sum_{u\in\mathcal{K}\backslash k}\mathbf{h}_k^{\mathrm{H}}\mathbf{F}_u\mathbf{h}_k \geq \sigma_k^2 + \frac{\delta_k^2}{\rho_k}, \quad \forall k, \tag{25b}$$

$$2\mu_k^{(i)}\sqrt{\sum_{j=1}^{K}\mathbf{h}_k^{\mathrm{H}}\mathbf{F}_j\mathbf{h}_k + \sigma_k^2}$$
$$- \big(\mu_k^{(i)}\big)^2 e_k \geq \frac{1}{\zeta_k(1-\rho_k)}, \quad \forall k, \tag{25c}$$

$$\gamma_k \leq 2^{R_k^{\max}} - 1, \quad \forall k, \tag{25d}$$

$$e_k \leq E_k^{\max}, \quad \forall k, \tag{25e}$$

$$0 \leq \rho_k \leq 1, \quad \forall k, \tag{25f}$$

$$\mathbf{F}_k \succeq 0, \quad \forall k. \tag{25g}$$

Note that (25) provides an approximate solution for (22) in the vicinity of $\{\nu_k^{(i)}, \mu_k^{(i)}\}$. Thus, by iteratively solving (25) while updating $\{\nu_k^{(i)}, \mu_k^{(i)}\}$ with the solution of current iteration, we can find a solution for (22) [39]. Moreover, for a fixed operating point $\{\nu_k^{(i)}, \mu_k^{(i)}\}$, the subproblem (25) can be efficiently solved using convex optimization tools, e.g., CVX [43].

For a given time slot t, let $\big\{\mathbf{F}_k^{\star}(t), \gamma_k^{\star}(t), e_k^{\star}(t), \rho_k^{\star}(t)\big\}_{\forall k}$ denote the solution obtained from (25). However, note that the achievable SINR (3) and the maximum harvested power (5) at k-th UE is computed by using actual beamforming vectors $\mathbf{f}_k^{\star}(t)$ and PS ratios $\rho_k^{\star}(t)$. Therefore, if $\mathbf{F}_k^{\star}(t)$ satisfies $\mathrm{Rank}\big(\mathbf{F}_k^{\star}(t)\big) = 1, \forall k \in \mathcal{K}$, we can write $\mathbf{F}_k^{\star}(t) = \mathbf{f}_k^{\star}(t)\mathbf{f}_k^{\star\,\mathrm{H}}(t)$, and $\mathbf{f}_k^{\star}(t)$ is a feasible solution to original problem (21). On the contrary, if $\mathrm{Rank}\big(\mathbf{F}_k^{\star}(t)\big) > 1$, an additional post-approximation procedure is required to obtain the beamforming vectors, which inevitably degrades

the achievable solution [41], [42]. For example, one possible rank-one approximation is obtained by simply setting $\{\mathbf{f}_k^{\star}(t)\}_{\forall k}$ to be proportional to the eigenvector $\mathbf{q}_k^1(t)$ of $\{\mathbf{F}_k^{\star}(t)\}_{\forall k}$ associated with the largest eigenvalue $\lambda_k^1(t)$, i.e., $\mathbf{f}_k^{\star}(t) = \sqrt{\varrho_k^{\star}(t)}\mathbf{q}_k^1(t), \forall k \in \mathcal{K}$, where ϱ_k is scaled to satisfy all the constraints in (25) [42]. Specifically, after $\{\mathbf{q}_k^1(t)\}_{\forall k}$ are obtained, (25) is modified by replacing $\mathbf{F}_k(t)$ with $\widetilde{\mathbf{F}}_k(t)$, and introducing additional constraints $\widetilde{\mathbf{F}}_k(t) = \varrho_k(t)\mathbf{q}_k^1(t)\mathbf{q}_k^{1\,\mathrm{H}}(t)$, and then solve the problem with optimization variables $\varrho_k, \forall k \in \mathcal{K}$ (we refer the reader to [42] and [41] for details). The joint optimization of beamformers and PS ratios, with the proposed SDR-FP based convex approximation, has been summarized in Algorithm 2.

Algorithm 2 SDR-FP Based Iterative Algorithm for (25)

---

1 Initialize with feasible starting point $\{\nu_k^{(0)}, \mu_k^{(0)}\}$, $\forall k$, and set $i = 1$

2 repeat

3 $\quad$ Solve (25) with $\{\nu_k^{(i-1)}, \mu_k^{(i-1)}\}$, and denote the local solution as $\big\{\mathbf{F}_k^{(i)}, \gamma_k^{(i)}, e_k^{(i)}, \rho_k^{(i)}\big\}$

4 $\quad$ Update $\nu_k^{(i)}$ using (23c) with $\big\{\mathbf{F}_k^{(i)}, \gamma_k^{(i)}\big\}$, and $\mu_k^{(i)}$ using (24c) with $\big\{\mathbf{F}_k^{(i)}, e_k^{(i)}\big\}$

5 $\quad$ Set $i = i + 1$

6 until convergence or for fixed number of iterations

B. Solution of (21) via SCA Framework

In this subsection, we employ the SCA framework [40], wherein the constraints (21b) and (21c) are successively upper-bounded with a sequence of convex subsets via first-order linear Taylor series approximations. The underlying convex subproblem is then iteratively solved until the desired convergence of the objective function. Note that, in contrast to the above-mentioned SDR-FP technique, here the optimized beamformers are obtained directly from the feasible solution, and no additional post-processing steps are required. The SCA based solutions have been widely used in many practical applications, e.g., spectrum sharing, energy efficiency, and multi-antenna interference coordination. For example, the SCA based linear Taylor series relaxation of the concave-convex fractional constraints is provided in our earlier work [2], [37]. In the following, the main steps are briefly reproduced.

1) Convex Approximation for Constraint (21b)*:* We start by rewriting SINR constraint (21b) as

$$\gamma_k \leq \frac{|\mathbf{h}_k^{\mathrm{H}}\mathbf{f}_k|^2}{\sum_{u\in\mathcal{K}\backslash k}|\mathbf{h}_k^{\mathrm{H}}\mathbf{f}_u|^2 + \sigma_k^2 + \frac{\delta_k^2}{\rho_k}}, \quad \forall k. \tag{26}$$

For compact representation, we define new functions as

$$G_k(\mathbf{f}_k, \gamma_k) \triangleq \frac{|\mathbf{h}_k^{\mathrm{H}}\mathbf{f}_k|^2}{\gamma_k}, \tag{27a}$$

$$I_k(\mathbf{F}, \rho_k) \triangleq \sum_{u\in\mathcal{K}\backslash k}|\mathbf{h}_k^{\mathrm{H}}\mathbf{f}_u|^2 + \sigma_k^2 + \frac{\delta_k^2}{\rho_k}, \tag{27b}$$

where $\mathbf{F} \triangleq [\mathbf{f}_1, \mathbf{f}_2, \ldots, \mathbf{f}_K]$. Hence, expression (26) can be equivalently written as

$$I_k(\mathbf{F}, \rho_k) - G_k(\mathbf{f}_k, \gamma_k) \leq 0, \quad \forall k. \tag{28}$$

Note that (27a) is a quadratic-over-linear function, and (27b) is a convex function with respect to the optimization variables, hence, the left-hand side (LHS) of (28) is a difference of convex functions [38, Ch. 3]. Thus, the linear convex approximation of the equivalent constraint (28) can be obtained by replacing $G_k(\mathbf{f}_k, \gamma_k)$ with its first-order Taylor series approximation around a fixed operating point $\{\mathbf{f}_k^{(i)}, \gamma_k^{(i)}\}$

$$\widetilde{G}_k(\mathbf{f}_k, \gamma_k, \mathbf{f}_k^{(i)}, \gamma_k^{(i)}) \triangleq 2\Re\left\{\frac{\mathbf{f}_k^{(i)\,\mathrm{H}}\mathbf{h}_k\mathbf{h}_k^{\mathrm{H}}}{\gamma_k^{(i)}}(\mathbf{f}_k - \mathbf{f}_k^{(i)})\right\}$$
$$+ \frac{|\mathbf{h}_k^{\mathrm{H}}\mathbf{f}_k^{(i)}|^2}{\gamma_k^{(i)}}\left(1 - \frac{\gamma_k - \gamma_k^{(i)}}{\gamma_k^{(i)}}\right). \tag{29}$$

2) Convex Approximation for Constraint (21c): To begin with, we rewrite expression (21c) as

$$\frac{e_k}{\zeta_k(1-\rho_k)} \leq \sum_{j=1}^{K} |\mathbf{h}_k^{\mathrm{H}}\mathbf{f}_j|^2 + \sigma_k^2, \quad \forall k. \tag{30}$$

For compact representation, we define new functions as

$$C_k(\rho_k) \triangleq \frac{1}{\zeta_k(1-\rho_k)}, \tag{31a}$$

$$S_k(\mathbf{F}, e_k) \triangleq \frac{\sum_{j=1}^{K} |\mathbf{h}_k^{\mathrm{H}}\mathbf{f}_j|^2 + \sigma_k^2}{e_k}. \tag{31b}$$

Hence, expression (30) can be rewritten as

$$C_k(\rho_k) - S_k(\mathbf{F}, e_k) \leq 0, \quad \forall k. \tag{32}$$

Observe that (31a) and (31b) are respectively convex and quadratic-over-linear functions with respect to the optimization variables. Hence, the LHS of (32) is again a difference of convex functions [38, Ch. 3]. Then, to provide the linear convex approximation of equivalent constraint (32), we replace $S_k(\mathbf{F})$ with its first-order linear Taylor series approximation around a fixed operating point $\{\mathbf{F}^{(i)}, e_k^{(i)}\}$

$$\widetilde{S}_k(\mathbf{F}, e_k, \mathbf{F}^{(i)}, e_k^{(i)})$$
$$\triangleq 2\sum_{j=1}^{K}\Re\left\{\mathbf{f}_j^{(i)\,\mathrm{H}}\mathbf{h}_k\mathbf{h}_k^{\mathrm{H}}(\mathbf{f}_j - \mathbf{f}_j^{(i)})\right\}$$
$$+ \frac{\sum_{j=1}^{K}|\mathbf{h}_k^{\mathrm{H}}\mathbf{f}_j^{(i)}|^2 + \sigma_k^2}{e_k^{(i)}}\left(1 - \frac{e_k - e_k^{(i)}}{e_k^{(i)}}\right). \tag{33}$$

3) Approximated Convex Subproblem: After replacing (21b) and (21c) with its linear Taylor series approximations (29) and (33), respectively, the problem (21) can be approximated as the following convex subproblem:

$$\min_{\substack{\{\mathbf{f}_k, \gamma_k, \\ e_k, \rho_k\}}} \quad V\sum_{k\in\mathcal{K}}\|\mathbf{f}_k\|^2 - \sum_{k\in\mathcal{K}}\omega_k(B_k^{\max} - B_k)e_k$$
$$- \sum_{k\in\mathcal{K}}(Q_k + A_k + Z_k)\log_2(1+\gamma_k) \tag{34a}$$

$$\text{s.t. } I_k(\mathbf{F}, \rho_k) - \widetilde{G}_k(\mathbf{f}_k, \gamma_k, \mathbf{f}_k^{(i)}, \gamma_k^{(i)}) \leq 0, \quad \forall k, \tag{34b}$$

$$C_k(\rho_k) - \widetilde{S}_k(\mathbf{F}, e_k, \mathbf{F}^{(i)}, e_k^{(i)}) \leq 0, \quad \forall k, \tag{34c}$$

$$\gamma_k \leq 2^{R_k^{\max}} - 1, \quad \forall k, \tag{34d}$$

$$e_k \leq E_k^{\max}, \quad \forall k, \tag{34e}$$

$$0 \leq \rho_k \leq 1, \quad \forall k. \tag{34f}$$

Note that the subproblem (34) provides an approximate solution in the proximity of a fixed operating point. Thus, by iteratively solving (34) with a convex optimization solver, e.g., CVX [43], and updating variables $\{\mathbf{f}_k^{(i)}, \gamma_k^{(i)}, e_k^{(i)}, \rho_k^{(i)}\}$ with the current SCA solution, as illustrated in Algorithm 3, we obtain a solution for problem (21).

Algorithm 3 SCA Based Iterative Algorithm for (34)

---

1 Initialize with feasible starting point
  $\{\mathbf{f}_k^{(0)}, \gamma_k^{(0)}, e_k^{(0)}, \rho_k^{(0)}\}$, $\forall k$, and set $i = 1$
2 repeat
3 | Solve (34) with $\{\mathbf{f}_k^{(i-1)}, \gamma_k^{(i-1)}, e_k^{(i-1)}, \rho_k^{(i-1)}\}$ and
    | denote the solution as $\{\mathbf{f}_k^{\star}, \gamma_k^{\star}, e_k^{\star}, \rho_k^{\star}\}$
4 | Update $\{\mathbf{f}_k^{(i)} = \mathbf{f}_k^{\star}\}$, $\{\gamma_k^{(i)} = \gamma_k^{\star}\}$, $\{e_k^{(i)} = e_k^{\star}\}$ and
    | $\{\rho_k^{(i)} = \rho_k^{\star}\}$
5 | Set $i = i + 1$
6 until convergence or for fixed number of iterations

V. DELAY-BOUNDED BATTERYLESS DEVICES

In this section, we study a special scenario of great practical significance, the case of batteryless UEs, which is key for self-sustainable and battery-free future wireless networks [3]. Delay bounded batteryless and low-power networks can play a crucial role for e.g., emergency networks and industrial automation scenarios, due to dense deployment and restricted human access.

As there is no battery in the user devices, the energy harvested from the RF received signals is immediately available to support the receiver operations in the current time slot [16], [17], e.g., based on the *harvest-use* strategy [4, Sec. III].[4] Moreover, the remainder of the extra harvested energy will be discarded by the user devices. Therefore, constraints (21d) and (21e) are no longer required for this specific SWIPT-enabled batteryless setup [16]. However, the receiver must be able to harvest an adequate amount of energy, i.e., to support its circuit power consumption and decoding operations on the downlink received data. Let $\ddot{e}_k(t)$ denote a (fixed) minimum harvested power QoS requirement of the k-th UE for seamless receiver operations during time slot t. In the following, time index t is omitted for notation brevity. Thereby, the problem (21) can be recast as

$$\min_{\{\mathbf{f}_k, \gamma_k, \rho_k\}} \quad V\sum_{k\in\mathcal{K}}\|\mathbf{f}_k\|^2$$
$$- \sum_{k\in\mathcal{K}}(Q_k + A_k + Z_k)\log_2(1+\gamma_k) \tag{35a}$$

---
[4]The harvested energy is temporarily stored in a built-in capacitor, which can be immediately used for receiver operations [4].

$$\text{s.t. } \gamma_k \leq \frac{\rho_k |\mathbf{h}_k{}^H \mathbf{f}_k|^2}{\rho_k \sum_{u \in \mathcal{K} \backslash k} |\mathbf{h}_k{}^H \mathbf{f}_u|^2 + \rho_k \sigma_k^2 + \delta_k^2}, \quad \forall k, \quad (35b)$$

$$\ddot{e}_k \leq \zeta_k (1 - \rho_k) \Big(\sum_{j=1}^K |\mathbf{h}_k{}^H \mathbf{f}_j|^2 + \sigma_k^2 \Big), \quad \forall k, \quad (35c)$$

$$0 \leq \rho_k \leq 1, \quad \forall k. \quad (35d)$$

Problem (35) is intractable due to the non-convex SINR constraint (35b), and the coupling between optimization variables $\{\mathbf{f}_k, \rho_k\}$ in expression (35b) and (35c).

We again adopt the SCA framework [40], wherein the non-convex constraints (35b) and (35c) are upper-bounded with their first-order Taylor series approximations. Note that (35b) is equivalent to (21b), and it can be handled as described in Section IV-B.1. Moreover, following the steps presented in Section IV-B.2, constraint (35c) can be addressed as follows.

To begin with, we rewrite expression (35c) as

$$\frac{\ddot{e}_k}{\zeta_k (1 - \rho_k)} \leq \sum_{j=1}^K |\mathbf{h}_k{}^H \mathbf{f}_j|^2 + \sigma_k^2, \quad \forall k. \quad (36)$$

For compact representation, we define new functions as

$$\ddot{C}_k(\rho_k) \triangleq \frac{\ddot{e}_k}{\zeta_k (1 - \rho_k)}, \quad (37a)$$

$$\ddot{S}_k(\mathbf{F}) \triangleq \sum_{j=1}^K |\mathbf{h}_k{}^H \mathbf{f}_j|^2 + \sigma_k^2. \quad (37b)$$

Hence, expression (36) can be equivalently rewritten as

$$\ddot{C}_k(\rho_k) - \ddot{S}_k(\mathbf{F}) \leq 0, \quad \forall k. \quad (38)$$

We can observe that both (37a) and (37b) are convex functions, and hence, the LHS of (38) is a difference of convex functions [38, Ch. 3]. We replace the quadratic function $\ddot{S}_k(\mathbf{F})$ with its first-order Taylor series approximation around a fixed operating point $\{\mathbf{F}^{(i)}\}$ as

$$\widetilde{\ddot{S}}_k(\mathbf{F}, \mathbf{F}^{(i)}) \triangleq \sum_{j=1}^K |\mathbf{h}_k{}^H \mathbf{f}_j^{(i)}|^2 + \sigma_k^2$$
$$+ 2 \sum_{j=1}^K \Re \Big\{ \mathbf{f}_j^{(i)\,H} \mathbf{h}_k \mathbf{h}_k{}^H \big(\mathbf{f}_j - \mathbf{f}_j^{(i)} \big) \Big\}. \quad (39)$$

Thereby, the problem (35) can be approximated as the following convex subproblem around a fixed operating point $\{\mathbf{f}_k^{(i)}, \gamma_k^{(i)}\}$

$$\min_{\{\mathbf{f}_k, \gamma_k, \rho_k\}} V \sum_{k \in \mathcal{K}} \|\mathbf{f}_k\|^2$$
$$- \sum_{k \in \mathcal{K}} (Q_k + A_k + Z_k) \log_2(1 + \gamma_k) \quad (40a)$$

$$\text{s.t. } \lambda_{k,1} : I_k(\mathbf{F}, \rho_k)$$
$$- \widetilde{G}_k(\mathbf{f}_k, \gamma_k, \mathbf{f}_k^{(i)}, \gamma_k^{(i)}) \leq 0, \quad \forall k, \quad (40b)$$

$$\lambda_{k,2} : \ddot{C}_k(\rho_k) - \widetilde{\ddot{S}}_k(\mathbf{F}, \mathbf{F}^{(i)}) \leq 0, \quad \forall k, \quad (40c)$$

$$\lambda_{k,3} : \rho_k \geq 0, \quad \forall k, \quad (40d)$$

$$\lambda_{k,4} : \rho_k \leq 1, \quad \forall k, \quad (40e)$$

where $\boldsymbol{\lambda}_k = [\lambda_{k,1}, \lambda_{k,2}, \lambda_{k,3}, \lambda_{k,4}]$ are non-negative Lagrange multipliers associated with each constraint. The role of the Lagrange multipliers will become clear in the following subsection. Note that subproblem (40) can be iteratively solved using standard convex optimization tools, e.g., CVX [43], as illustrated in Algorithm 4.

Algorithm 4 SCA Based Iterative Algorithm for (40)

1 Initialize with feasible starting point
 $\{\mathbf{f}_k^{(0)}, \gamma_k^{(0)}, \rho_k^{(0)}\}$, $\forall k$, and set $i = 1$
2 repeat
3   Solve (40) with $\{\mathbf{f}_k^{(i-1)}, \gamma_k^{(i-1)}, \rho_k^{(i-1)}\}$ and denote
     the solution as $\{\mathbf{f}_k^\star, \gamma_k^\star, \rho_k^\star\}$
4   Update $\{\mathbf{f}_k^{(i)} = \mathbf{f}_k^\star\}$, $\{\gamma_k^{(i)} = \gamma_k^\star\}$ and $\{\rho_k^{(i)} = \rho_k^\star\}$
5   Set $i = i + 1$
6 until convergence or for fixed number of iterations

A. Solution of (40) via KKT Conditions

Herein, we also provide a low-complexity iterative algorithm that does not rely on generic convex solvers. Specifically, we tackle (40) by iteratively solving a system of closed-form KKT optimality conditions [38, Ch. 5.5]. After some algebraic manipulations, we obtain the Lagrangian $\mathcal{L}(\mathbf{F}, \gamma_k, \rho_k, \boldsymbol{\lambda}_k)$ of (40) as detailed in (41), shown at the bottom of the next page. Next, by differentiating (41) with respect to primal optimization variables $\{\mathbf{f}_k, \gamma_k, \rho_k\}$, we obtain the stationarity conditions for (40), given by

$$\nabla_{\mathbf{f}_k} : \mathbf{f}_k{}^H \Big(V \mathbb{I} + \sum_{u \in \mathcal{K} \backslash k} \lambda_{u,1} \mathbf{h}_u \mathbf{h}_u{}^H \Big)$$
$$= \lambda_{k,1} \frac{\mathbf{f}_k^{(i)\,H} \mathbf{h}_k \mathbf{h}_k{}^H}{\gamma_k^{(i)}} + \mathbf{f}_k^{(i)\,H} \sum_{j=1}^K \lambda_{j,2} \mathbf{h}_j \mathbf{h}_j{}^H, \quad (42a)$$

$$\nabla_{\gamma_k} : \frac{Q_k + A_k + Z_k}{1 + \gamma_k} = \lambda_{k,1} \frac{|\mathbf{h}_k{}^H \mathbf{f}_k^{(i)}|^2}{(\gamma_k^{(i)})^2}, \quad (42b)$$

$$\nabla_{\rho_k} : \lambda_{k,1} \frac{\delta_k^2}{\rho_k^2} = \lambda_{k,2} \frac{\ddot{e}_k}{\zeta_k (1 - \rho_k)^2} + (\lambda_{k,4} - \lambda_{k,3}). \quad (42c)$$

Further, in addition to primal-dual feasibility, the KKT conditions include the complementary slackness, defined as

$$\lambda_{k,1} \geq 0; \; \lambda_{k,1} \big\{ I_k(\mathbf{F}, \rho_k)$$
$$- \widetilde{G}_k(\mathbf{f}_k, \gamma_k, \mathbf{f}_k^{(i)}, \gamma_k^{(i)}) \big\} = 0, \quad \forall k, \quad (43a)$$

$$\lambda_{k,2} \geq 0; \; \lambda_{k,2} \big\{ \ddot{C}_k(\rho_k) - \widetilde{\ddot{S}}_k(\mathbf{F}, \mathbf{F}^{(i)}) \big\} = 0, \quad \forall k, \quad (43b)$$

$$\lambda_{k,3} \geq 0; \; \lambda_{k,3} \big\{ 0 - \rho_k \big\} = 0, \quad \forall k, \quad (43c)$$

$$\lambda_{k,4} \geq 0; \; \lambda_{k,4} \big\{ \rho_k - 1 \big\} = 0, \quad \forall k. \quad (43d)$$

Note that the associated dual variable $\{\boldsymbol{\lambda}_k\}$ is strictly positive only when the constraint is tight. Specifically, setting $\lambda_{k,3} > 0$ would imply $\rho_k = 0$. However, in such a case, expression (27b) would become infeasible. Similarly, $\lambda_{k,4} > 0$ results in $\rho_k = 1$, and it would make expression (37a) infeasible. Thus, we can conclude that constraints (40d) and (40e) are not tight at a feasible solution of (40), i.e., $0 < \rho_k < 1$ and

$\lambda_{k,3} = \lambda_{k,3} = 0, \forall k \in \mathcal{K}$. Next, let us assume the Lagrange multipliers $\lambda_{k,1} > 0$ and $\lambda_{2,1} > 0$, $\forall k \in \mathcal{K}$. Then, after some algebraic manipulations of expressions (42) and (43), the closed-form steps in the iterative method are

$$\tilde{\mathbf{f}}_k = \left(V\mathbb{I} + \sum_{u\in\mathcal{K}\setminus k} \lambda_{u,1}^{(i-1)} \mathbf{h}_u \mathbf{h}_u^{\mathsf{H}} \right)^{-1} \times \left\{ \frac{\lambda_{k,1}^{(i-1)}}{\gamma_k^{(i-1)}} \mathbf{h}_k \mathbf{h}_k^{\mathsf{H}} \mathbf{f}_k^{(i-1)} \right.$$
$$\left. + \sum_{j=1}^K \lambda_{j,2}^{(i-1)} \mathbf{h}_j \mathbf{h}_j^{\mathsf{H}} \mathbf{f}_k^{(i-1)} \right\}, \tag{44a}$$

$$\mathbf{f}_k^{(i)} = \mathbf{f}_k^{(i-1)} + \beta(\tilde{\mathbf{f}}_k - \mathbf{f}_k^{(i-1)}), \tag{44b}$$

$$\rho_k^{(i)} = 1 - \frac{\ddot{e}_k}{\zeta_k} \left\{ 2 \sum_{j=1}^K \Re\left\{ \mathbf{f}_j^{(i-1)\,\mathsf{H}} \mathbf{h}_k \mathbf{h}_k^{\mathsf{H}} (\mathbf{f}_j^{(i)} - \mathbf{f}_j^{(i-1)}) \right\} \right.$$
$$\left. + \sum_{j=1}^K |\mathbf{h}_k^{\mathsf{H}} \mathbf{f}_j^{(i-1)}|^2 + \sigma_k^2 \right\}^{-1}, \tag{44c}$$

$$\gamma_k^{(i)} = 2\gamma_k^{(i-1)} + \left\{ 2\Re\left\{ \frac{\mathbf{f}_k^{(i-1)\,\mathsf{H}} \mathbf{h}_k \mathbf{h}_k^{\mathsf{H}}}{\gamma_k^{(i-1)}} (\mathbf{f}_k^{(i)} - \mathbf{f}_k^{(i-1)}) \right\} \right.$$
$$\left. - \sum_{u\in\mathcal{K}\setminus k} |\mathbf{h}_k^{\mathsf{H}} \mathbf{f}_u^{(i)}|^2 - \sigma_k^2 - \frac{\delta_k^2}{\rho_k^{(i)}} \right\} \frac{(\gamma_k^{(i-1)})^2}{|\mathbf{h}_k^{\mathsf{H}} \mathbf{f}_k^{(i-1)}|^2}, \tag{44d}$$

$$\lambda_{k,1}^{(i)} = \frac{(Q_k + A_k + Z_k)(\gamma_k^{(i-1)})^2}{(1 + \gamma_k^{(i)})|\mathbf{h}_k^{\mathsf{H}} \mathbf{f}_k^{(i-1)}|^2}, \tag{44e}$$

$$\lambda_{k,2}^{(i)} = \frac{\zeta_k \delta_k^2 \lambda_{k,1}^{(i-1)} (1 - \rho_k^{(i-1)})^2}{\ddot{e}_k (\rho_k^{(i-1)})^2}, \tag{44f}$$

where β is a positive step size, i.e., $0 < \beta \leq 1$. It is worth highlighting that the SWIPT beamformer design (44a) inherently has a multicast structure due to EH from RF received signals [15]. Specifically, the dual variables $\{\lambda_{k,1}\}$ and $\{\lambda_{k,2}\}$ control the balance between information unicasting and energy multicasting to each user, respectively. Note that to avoid separate outer and inner loop updates, and hence, to speed up the convergence, the fixed operating point $\{\mathbf{f}_k^{(i)}, \gamma_k^{(i)}\}$ is also heuristically updated in each iteration along with the associated Lagrange multipliers. Thus, in general, the monotonic convergence can not be guaranteed. However, to improve the convergence behaviour, we employ the best response (BR) method to regularize the beamformer update in expression (44b). In Section VI, we show via a numerical example that, with a proper choice of β in (44b), a monotonic convergence of the objective function can be achieved with a fairly small number of iterations. The proposed method

consists of iteratively solving a system of closed-form KKT equations as summarized in Algorithm 5.

Algorithm 5 KKT Based Iterative Algorithm for (40)

---

1 Initialize with feasible starting point
   $\{\mathbf{f}_k^{(0)}, \gamma_k^{(0)}, \rho_k^{(0)}, \boldsymbol{\lambda}_k^{(0)}\}$, $\forall k$, and set $i = 1$

2 repeat

3   Solve $\tilde{\mathbf{f}}_k$ from (44a) and update $\mathbf{f}_k^{(i)}$ using (44b)

4   Compute variables $\rho_k^{(i)}, \gamma_k^{(i)}$ from (44c), (44d), respectively

5   Obtain Lagrange multipliers $\lambda_{k,1}^{(i)}, \lambda_{k,2}^{(i)}$ from (44e), (44f), respectively

6   Set $i = i + 1$

7 until convergence or for fixed iterations

VI. SIMULATION RESULTS

In this section, we provide numerical examples to assess the performance of the proposed algorithms for joint transmit beamformers and receive PS ratios optimization. We consider a SWIPT system with $K = 2$ UEs being served by a BS equipped with a uniform linear array (ULA) of $N_t = 8$ antenna elements. For simplicity, we assume identical parameters for all UEs. Specifically, we set noise variance $\delta_k^2 = -50$ dBm and $\sigma_k^2 = -70$ dBm; EH conversion efficiency $\zeta_k = 0.8$, $\forall t, k$ [17]. Without loss of generality, we assume maximum battery capacity $B_k^{\max} = 10$ Joules; fixed energy consumption $P_k^{\text{cir}} = 0$ dBm; energy efficiency of decoder circuit $\vartheta_k^d = 0.5$ [Joules/bit]; normalized frame duration $T_f = 1$; and scaling factor $\omega_k = 150$, $\forall t, k$. Further, we consider a Poisson arrival process $A_k \sim \text{Pois}(\alpha)$ with allowable queue backlog $Q_k^{\text{th}} = 5$ bits and tolerable violation probability $\epsilon = 10\%$ in problem (12) [37]. We set the fixed minimum harvested power requirement $\ddot{e}_k(t) = 10$ dBm, $\forall t, k$ in problem (35). Finally, we set the step size $\beta = 0.25$ in expressions (44b). If not mentioned otherwise, we consider problem (12) and all the results are averaged over randomly generated 3000 channel realizations.

We consider uncorrelated Rician fading to model the radio propagation channel. Specifically, the channel $\mathbf{h}_k \in \mathbb{C}^{N_t \times 1}$ of k-th UE consists of a deterministic Line-of-Sight (LoS) path $\mathbf{h}_k^{\text{LoS}}$ and a spatially uncorrelated non-LoS (NLoS) path $\mathbf{h}_k^{\text{NLoS}}$, such that

$$\mathbf{h}_k(t) = \sqrt{\frac{\kappa}{1+\kappa}} \mathbf{h}_k^{\text{LoS}}(t) + \sqrt{\frac{1}{1+\kappa}} \mathbf{h}_k^{\text{NLoS}}(t), \quad \forall t, k, \tag{45}$$

$$\mathfrak{L}(\mathbf{F}, \gamma_k, \rho_k, \boldsymbol{\lambda}_k) = \sum_{k\in\mathcal{K}} \left[V\|\mathbf{f}_k\|^2 - (Q_k + A_k + Z_k)\log_2(1 + \gamma_k) + \sum_{u\in\mathcal{K}\setminus k} \lambda_{u,1} |\mathbf{h}_u^{\mathsf{H}} \mathbf{f}_k|^2 \right.$$
$$+ \lambda_{k,1} \left\{ \sigma_k^2 + \frac{\delta_k^2}{\rho_k} - 2\Re\left\{ \frac{\mathbf{f}_k^{(i)\,\mathsf{H}} \mathbf{h}_k \mathbf{h}_k^{\mathsf{H}}}{\gamma_k^{(i)}} (\mathbf{f}_k - \mathbf{f}_k^{(i)}) \right\} - 2\frac{|\mathbf{h}_k^{\mathsf{H}} \mathbf{f}_k^{(i)}|^2}{\gamma_k^{(i)}} + \gamma_k \frac{|\mathbf{h}_k^{\mathsf{H}} \mathbf{f}_k^{(i)}|^2}{(\gamma_k^{(i)})^2} \right\} + \lambda_{k,2} \left\{ \left(\frac{1}{1-\rho_k}\right)\frac{\ddot{e}_k}{\zeta_k} \right\}$$
$$\left. - 2\sum_{j=1}^K \lambda_{j,2} \Re\left\{ \mathbf{f}_k^{(i)\,\mathsf{H}} \mathbf{h}_j \mathbf{h}_j^{\mathsf{H}} (\mathbf{f}_k - \mathbf{f}_k^{(i)}) \right\} - \lambda_{k,2} \left\{ \sum_{j=1}^K |\mathbf{h}_k^{\mathsf{H}} \mathbf{f}_j^{(i)}|^2 + \sigma_k^2 \right\} + \rho_k\{\lambda_{k,4} - \lambda_{k,3}\} - \lambda_{k,4} \right]. \tag{41}$$
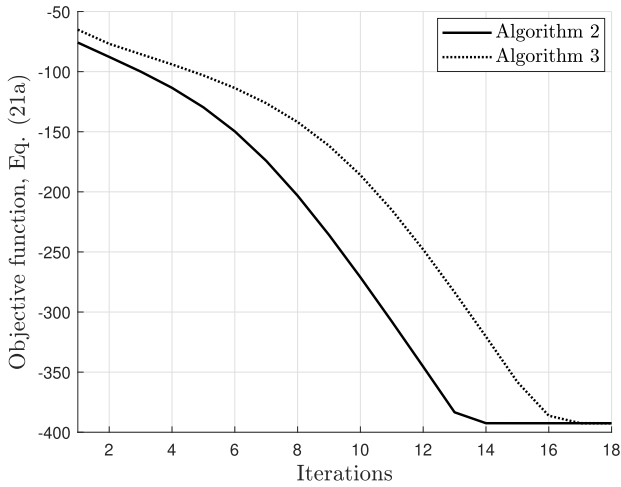
Fig. 3. Convergence behavior of Algorithm 2 and Algorithm 3 for (21) with $V = 1$ and mean arrival $\alpha = 3$.

Fig. 4. The data queue backlog performance with $V = 1$ and different mean arrivals.

where κ is the Rician factor. We set $\kappa = 5$ dB unless stated otherwise. Moreover, the NLoS component is modeled independently for each time slot t using Rayleigh fading with the path-loss of -40 dB. Meanwhile, the LoS component follows the standard far-field ULA model, i.e., $\mathbf{h}_k^{\text{LoS}}(t) = \sqrt{10^{-4}}[1, \ e^{-\mathrm{j}\pi \sin(\theta_k(t))}, \ldots, e^{-\mathrm{j}(N_t-1)\pi \sin(\theta_k(t))}]^{\mathbf{T}}$, where $\theta_k(t)$ is the azimuth angle of k-th UE during time slot t relative to the boresight of the BS antenna array. The azimuth angles $\theta_k(t) \in [-\pi/2, \ \pi/2]$, $\forall t, k$, are randomly generated.

A. Convergence and Complexity Analysis

First, we investigate the convergence behavior of the proposed iterative algorithms for a given randomly generated channel realization. Note that the solution of (21), both in Algorithm 2 and Algorithm 3, is obtained directly from the convex optimization toolbox SeDuMi [43]. Further, the per-iteration computational complexity is dominated by the downlink beamformer optimization step and scales exponentially with the length of the beamforming vector N_t. It can be observed from Fig. 3 that the SDR-FP based iterative Algorithm 2 provides faster convergence in terms of the required approximation point updates. The interior point methods are usually adopted to solve SDP formulations, and each iteration requires $\mathcal{O}\big((K + N_t^2)^{3.5}\big)$ arithmetic operations [16], [44], [45, Sec. III]. Moreover, Algorithm 2 also requires additional post-approximation procedures to recover the rank-one beamforming vectors (see Section IV-A for more details). On the contrary, the SCA based iterative Algorithm 3 attains the feasible solution without any additional steps after the convergence. The approximated convex problems can be efficiently solved as a sequence of SOCP, and the worst-case computational complexity of each iteration is $\mathcal{O}\big((K + N_t)^{3.5}\big)$ [17], [44]. Note that both solutions exactly coincide, implying also that the Algorithm 2 yields a rank-one solution for the reformulated problem (12) in this particular scenario with the above considered setup configurations. However, the SDR-based optimization becomes expensive, potentially much more than SCA framework, as the number of transmit antennas N_t at
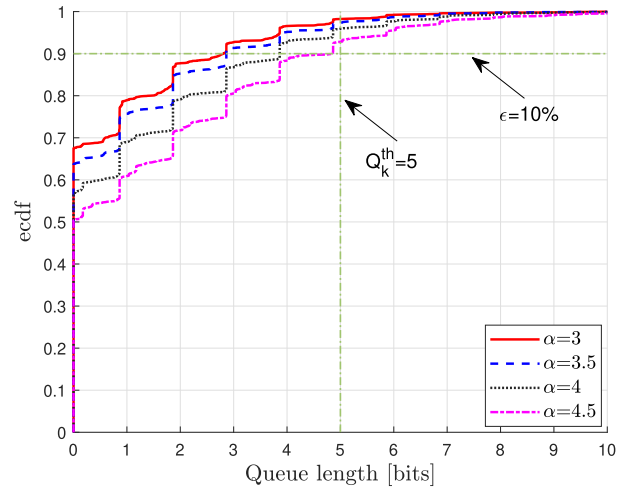
the BS increases (e.g., matrix $\{\mathbf{F}_k\}_{\forall k}$). Therefore, Algorithm 2 can be useful for delay-constrained devices with sufficient processing capabilities, while Algorithm 3 can be applied to hardware-constrained devices to produce a more computationally efficient solution.

B. Impact of Parameter V and Mean Arrival Rate α

Herein, we investigate the impact of different mean arrival rate α and trade-off parameter V on the achievable system performance. First, we set $V = 1$ and illustrate the empirical cumulative distribution function (ecdf) of the queue backlogs in Fig. 4. It can be concluded that irrespective of the mean arrival α, the proposed method ensures the maximum queue backlogs of each user k (i.e., $Q_k^{\text{th}} = 5$) within tolerable violation probability $\epsilon = 10\%$. Thus, the proposed convex relaxations to (12) still allow to satisfy the desired user-specific latency requirements (i.e., probabilistic queue backlog constraint (12b) is met). Note that similar performance trends can be obtained for different values of parameter V, but this is not illustrated due to space limitations.

Next, we examine the impact of different values of the trade-off parameter V on the average transmit power of the BS and the average harvested power at the receiver in Fig. 5 and Fig. 6, respectively. The result in Fig. 5 shows that the sum-power decreases with an increasing V. This is an expected behavior since V can be anticipated as a scaling factor for the sum-power objective function (see expression (21a) for details). Thus, higher values of V linearly emphasize the minimization of the BS transmit power over the sum of network queue backlogs and spare battery capacity until/unless the queues length becomes substantially larger than the sum-power objective value. Furthermore, we can observe that the BS sum-power significantly increases with the mean arrival rate. This is mainly due to the fact that the increase in the network queue backlogs (6) enforces downlink transmission with higher data rates to reduce users' queues, e.g., at the cost of consuming more energy, and thus, requiring higher BS transmit powers to quickly recharge the devices. Note that with the increasing
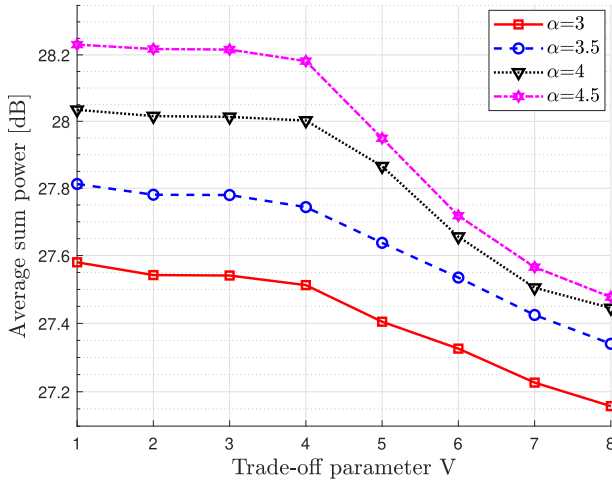
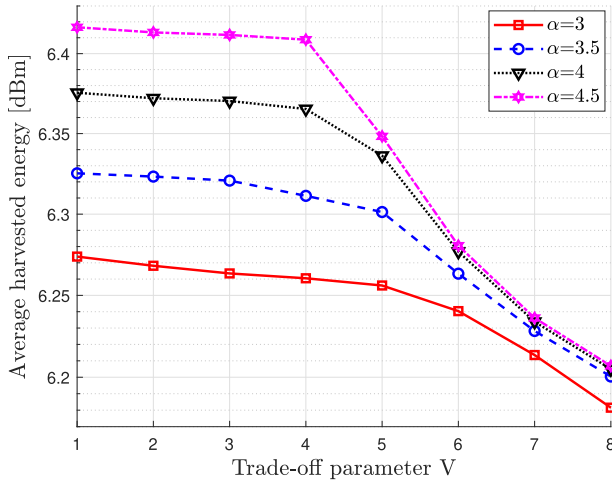Fig. 5. The BS average transmit power with increasing V and different mean arrivals.

Fig. 7. The dynamics of network queues with $V \in \{1,8\}$ and mean arrival $\alpha = 3$.

Fig. 6. The receiver average harvested energy with increasing V and different mean arrivals.

Fig. 8. The dynamics of virtual queues with $V \in \{1,8\}$ and mean arrival $\alpha = 3$.

interplay among network queue length, BS transmit power, and receiver spare battery capacity, as can be seen from Fig. 4−Fig. 6.

C. Network and virtual Queue Dynamics

Fig. 7 and Fig. 8 respectively show the dynamics of network queue backlogs $\{Q_k(t)\}$ and associated virtual queue $\{Z_k(t)\}$ over time with parameter $V = \{1,8\}$ for a given UE. It can be observed that the time dynamics of queues include a transient state and a steady state. Furthermore, the steady state is only attained after accumulating certain backlogs in the associated virtual queues $\{Z_k(t)\}$ as shown in Fig. 8. Thus, until/unless the virtual queue reaches a certain value at which it gets saturated (e.g., around $t = \{26,34\}$ for $V = \{1,8\}$), only then the actual network queue oscillate, so as the probabilistic queue length constraint $\Pr\{Q_k(t) \geq Q_k^{\text{th}}\} \leq \epsilon$ is satisfied, i.e., to achieve the probabilistic delay requirements (12b). This is mainly because of the negative drift property of the Lyapunov function [35, Ch. 4.4]. Specifically, the stability of associated virtual queues $\{Z_k(t)\}$ strictly ensures that the network queues are bounded [35, Th. 2.5], which allows achieving the desired user-specific queue backlogs performance.

V and α, it also becomes more stringent to satisfy the user-specific latency constraints (12b), as will become clear in the following.

Fig. 6 illustrates that the energy harvested at the receiver decreases with the increase of V. This is mainly due to the decrease in the transmit power of the BS with an increasing V, as also shown in Fig. 5. Note that a downlink transmission with less power leads, in general, to relatively less harvesting opportunities at the receivers. Furthermore, we can observe that the harvested power increases with the mean arrival rate. Specifically, with the increasing network queue backlogs (6), the BS attempts to increase the maximum downlink supported rates (10). Thus, the UEs consume significant energy resources to support their current data decoding operations (9), which eventually leads to greater EH requirements in subsequent time slots due to less available spare battery capacity (refer to Section II-C for more details). In this regard, our proposed virtual battery queue with the scaling on spare battery capacity (15) enforces more stringent EH requirements at the UEs to quickly recharge them and also stabilize the time-average battery queues (8). All in all, there is a strong
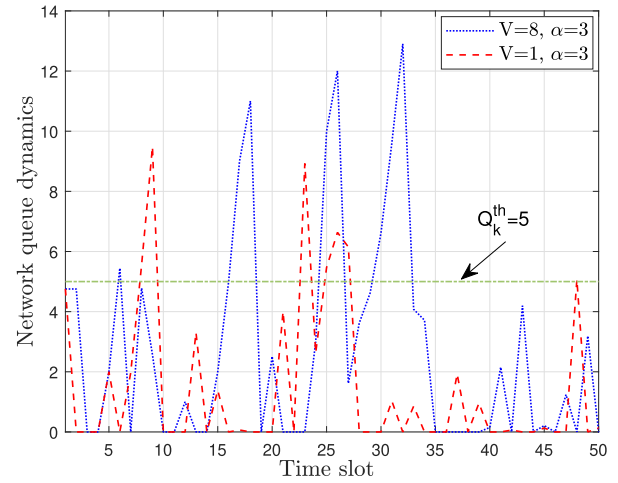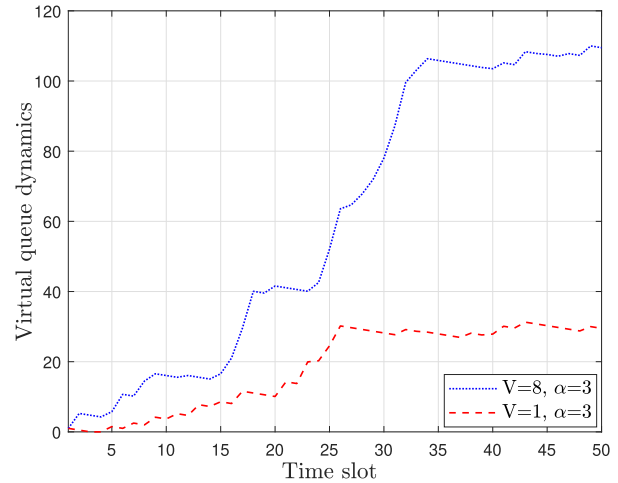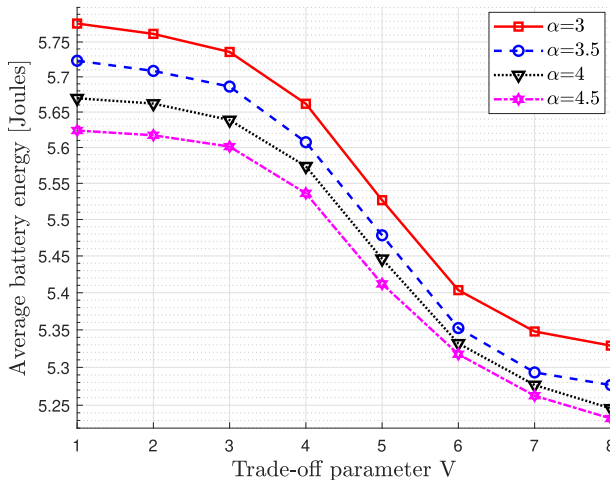
Fig. 9. The receiver average battery energy with increasing V and different mean arrivals.

Fig. 11. Convergence behavior of Algorithm 4 and Algorithm 5 for (35) with $V = 1$ and mean arrival $\alpha = 3$.

Fig. 10. The ecdf of battery charge levels with $V \in \{1, 8\}$ and mean arrival $\alpha = 3$.

Fig. 12. The queue backlog performance for different EH requirement with $V = 1$ and mean arrival $\alpha = 3$.

D. Receiver Battery Dynamics

Next, we examine the performance of receiver battery capacity in Fig. 9 and Fig. 10. It can be concluded from Fig. 9 that the average battery capacity decreases with an increasing V, mainly due to the decrease in BS transmit power and corresponding less harvesting opportunities at the receiver. As an example, by decreasing the parameter $V = 8$ to $V = 1$, the minimum battery charge level of a given UE is improved from $B_k = 1.45$ Joules to $B_k = 3.1$ Joules, as shown in Fig. 10. However, the average battery capacity remains somewhat similar with different mean arrival rates. This is due to the fact that the arrival with a higher rate enforces higher BS transmit power, and thus more harvested energy at the receiver (see Fig. 6) to support the more energy-demanding receive decoding process. Specifically, with increasing arrivals, the battery is quickly recharged to support the receivers' operation, and thus the battery level remains fairly stable.

To summarize, even after the proposed relaxations to problem (12), the solution still allows to satisfy the desired user-specific latency and maximum EH requirements. That is, constraints (12b)-(12e) are strictly met with the minimum BS transmit power. Thus, with the proposed dynamic control algorithm and suitable parameterization of drift-plus-penalty
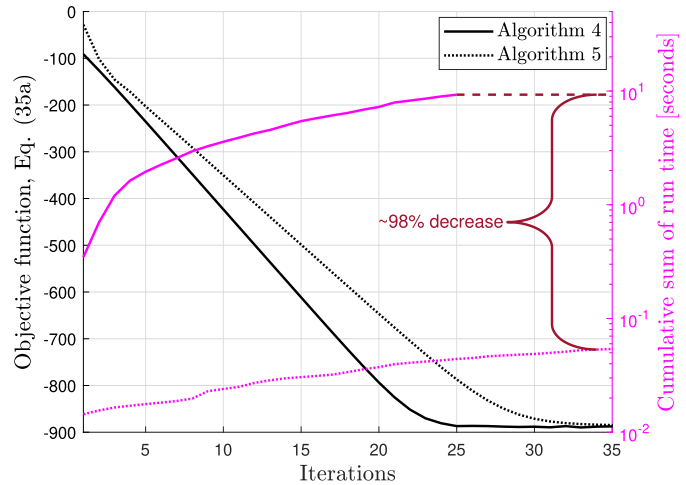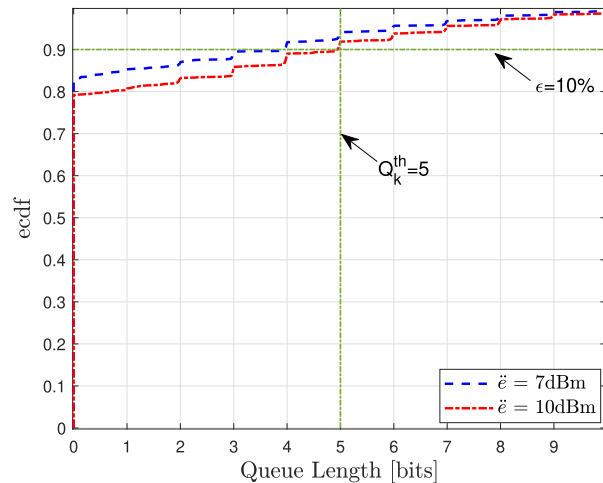
functions, one can easily handle the network queue backlogs, optimize the BS transmit power, and the receivers' battery charge level, while ensuring the user-specific latency and EH requirements of, e.g., industrial-grade delay bounded critical applications for factory automation scenarios.

E. Delay-Bounded Batteryless Devices

For the special scenario of delay bounded SWIPT-enabled batteryless receivers, we illustrate in Fig. 11 the run time and the convergence performance of Algorithm 4 and Algorithm 5 for solving problem (35). Note that different from the SCA based iterative approach in Algorithm 4, the solution of Algorithm 5 is based on an iterative evaluation of closed-form KKT expressions (44), thus, it does not rely on generic convex solvers. We can observe that the solution via Algorithm 5 achieves superior performance to Algorithm 4, e.g., around 98% improvement in the run time performance. Further, the computational complexity is mainly dominated by expression (44a), which consists of matrix multiplication and inverse operations. Hence, each iteration requires $\mathcal{O}(N_t^{2.37})$ arithmetic operations using, e.g., Coppersmith–Winograd algorithm [46], [38, Appendix C]. Thus, Algorithm 5 provides more practical, latency-conscious, and computationally efficient implementations. At this point, it is worth highlighting that a KKT based

closed-form iterative method may not be attained for (12) due to underlying complexity, coupling among optimization variables, and temporally correlated user-specific battery energy and EH constraints.

Finally, Fig. 12 illustrates the user-specific latency performance for different minimum harvested power requirements with the trade-off parameter $V = 1$ and mean arrival rate $\alpha = 3$. The result shows that, irrespective of the fixed harvested power constraint (35c), our proposed method ensures the maximum backlogs of each user k (i.e., $Q_k^{\text{th}} = 5$) within the allowable violation probability $\epsilon = 10\%$. Thus, the proposed convex relaxations to problem (35) still allow to satisfy the desired latency requirements. The other numerical examples are omitted due to space limitation, but similar performance trends can easily be obtained for (35) [1], [2].

VII. CONCLUSION

In this paper, we considered a PS based SWIPT system and provided a joint optimization of transmit beamforming vectors and receive PS ratios, while accounting for the limited battery energy at each UE. Specifically, we considered a long-term average BS transmit power minimization problem concurrently satisfying the user-specific latency and maximum EH requirements. The proposed radio resource allocation schemes efficiently avoid the receivers' battery depletion phenomenon by preemptively incorporating the spare battery capacity and EH fluctuations in a time dynamic mobile access network. To provide a tractable solution, we employed the Lyapunov optimization framework, and provided an online dynamic control algorithm to obtain a series of per-time slot deterministic subproblems. Furthermore, the coupled and non-convex constraints were handled by applying the techniques of SDR-FP and SCA framework. A closed-form iterative algorithm was designed by solving a system of KKT optimality conditions for a special case of delay bounded batteryless UEs. The simulation results manifested the robustness of the proposed design to realize an energy-efficient SWIPT system for industrial-grade delay bound applications.

REFERENCES

[1] D. Kumar, O. L. A. Lopez, A. Tolli, and S. Joshi, "Latency-aware joint transmit beamforming and receive power splitting for SWIPT systems," in *Proc. IEEE 32nd Annu. Int. Symp. Pers., Indoor Mobile Radio Commun. (PIMRC)*, Sep. 2021, pp. 490–494.

[2] D. Kumar, O. L. Alcaraz Lopez, S. Joshi, and A. Tolli, "Latency constrained simultaneous wireless information and power transfer," in *Proc. 17th Int. Symp. Wireless Commun. Syst. (ISWCS)*, Sep. 2021, pp. 1–6.

[3] O. L. A. López, H. Alves, R. D. Souza, S. Montejo-Sánchez, E. M. G. Fernández, and M. Latva-Aho, "Massive wireless energy transfer: Enabling sustainable IoT toward 6G era," *IEEE Internet Things J.*, vol. 8, no. 11, pp. 8816–8835, Jun. 2021.

[4] M.-L. Ku, W. Li, Y. Chen, and K. J. R. Liu, "Advances in energy harvesting communications: Past, present, and future challenges," *IEEE Commun. Surveys Tuts.*, vol. 18, no. 2, pp. 1384–1412, 2nd Quart. 2016.

[5] K. W. Choi et al., "Simultaneous wireless information and power transfer (SWIPT) for Internet of Things: Novel receiver design and experimental validation," *IEEE Internet Things J.*, vol. 7, no. 4, pp. 2996–3012, Apr. 2020.

[6] B. Clerckx, R. Zhang, R. Schober, D. W. K. Ng, D. I. Kim, and H. V. Poor, "Fundamentals of wireless information and power transfer: From RF energy harvester models to signal and system designs," *IEEE J. Sel. Areas Commun.*, vol. 37, no. 1, pp. 4–33, Jan. 2019.

[7] R. Zhang and C. K. Ho, "MIMO broadcasting for simultaneous wireless information and power transfer," *IEEE Trans. Wireless Commun.*, vol. 12, no. 5, pp. 1989–2001, May 2013.

[8] X. Zhou, R. Zhang, and C. K. Ho, "Wireless information and power transfer: Architecture design and rate-energy tradeoff," *IEEE Trans. Commun.*, vol. 61, no. 11, pp. 4754–4767, Nov. 2013.

[9] M. Sinaie, P.-H. Lin, A. Zappone, P. Azmi, and E. A. Jorswieck, "Delay-aware resource allocation for 5G wireless networks with wireless power transfer," *IEEE Trans. Veh. Technol.*, vol. 67, no. 7, pp. 5841–5855, Jul. 2018.

[10] X. Lu, I. Flint, D. Niyato, N. Privault, and P. Wang, "Self-sustainable communications with RF energy harvesting: Ginibre point process modeling and analysis," *IEEE J. Sel. Areas Commun.*, vol. 34, no. 5, pp. 1518–1535, May 2016.

[11] X. Lu, P. Wang, D. Niyato, D. I. Kim, and Z. Han, "Wireless networks with RF energy harvesting: A contemporary survey," *IEEE Commun. Surveys Tuts.*, vol. 17, no. 2, pp. 757–789, 2nd Quart., 2015.

[12] A. Ikhlef, "Optimal MIMO multicast transceiver design for simultaneous information and power transfer," *IEEE Commun. Lett.*, vol. 18, no. 12, pp. 2153–2156, Dec. 2014.

[13] J. Xu, L. Liu, and R. Zhang, "Multiuser MISO beamforming for simultaneous wireless information and power transfer," *IEEE Trans. Signal Process.*, vol. 62, no. 18, pp. 4798–4810, Sep. 2014.

[14] J. Park and B. Clerckx, "Joint wireless information and energy transfer in a K-user MIMO interference channel," *IEEE Trans. Wireless Commun.*, vol. 13, no. 10, pp. 5781–5796, Oct. 2014.

[15] S. Gautam, E. Lagunas, S. Chatzinotas, and B. Ottersten, "Feasible point pursuit and successive convex approximation for transmit power minimization in SWIPT-multigroup multicasting systems," *IEEE Trans. Green Commun. Netw.*, vol. 5, no. 2, pp. 884–894, Jun. 2021.

[16] Q. Shi, L. Liu, W. Xu, and R. Zhang, "Joint transmit beamforming and receive power splitting for MISO SWIPT systems," *IEEE Trans. Wireless Commun.*, vol. 13, no. 6, pp. 3269–3280, Jun. 2014.

[17] Q. Shi, W. Xu, T. Chang, Y. Wang, and E. Song, "Joint beamforming and power splitting for MISO interference channel with SWIPT: An SOCP relaxation and decentralized algorithm," *IEEE Trans. Signal Process.*, vol. 62, no. 23, pp. 6194–6208, Dec. 2014.

[18] H. Zhang, A. Dong, S. Jin, and D. Yuan, "Joint transceiver and power splitting optimization for multiuser MIMO SWIPT under MSE QoS constraints," *IEEE Trans. Veh. Technol.*, vol. 66, no. 8, pp. 7123–7135, Aug. 2017.

[19] A. Dong, H. Zhang, D. Wu, and D. Yuan, "QoS-constrained transceiver design and power splitting for downlink multiuser MIMO SWIPT systems," in *Proc. IEEE Int. Conf. Commun. (ICC)*, May 2016, pp. 1–6.

[20] B. Xu, Y. Zhu, and R. Zhang, "Optimized power allocation for interference channel with SWIPT," *IEEE Wireless Commun. Lett.*, vol. 5, no. 2, pp. 220–223, Apr. 2016.

[21] S. Timotheou, I. Krikidis, G. Zheng, and B. Ottersten, "Beamforming for MISO interference channels with QoS and RF energy transfer," *IEEE Trans. Wireless Commun.*, vol. 13, no. 5, pp. 2646–2658, May 2014.

[22] Z. Zong, H. Feng, F. R. Yu, N. Zhao, T. Yang, and B. Hu, "Optimal transceiver design for SWIPT in K-user MIMO interference channels," *IEEE Trans. Wireless Commun.*, vol. 15, no. 1, pp. 430–445, Jan. 2016.

[23] Q. Shi, C. Peng, W. Xu, M. Hong, and Y. Cai, "Energy efficiency optimization for MISO SWIPT systems with zero-forcing beamforming," *IEEE Trans. Signal Process.*, vol. 64, no. 4, pp. 842–854, Feb. 2016.

[24] J. Rubio and A. Pascual-Iserte, "Energy-aware broadcast multiuser-MIMO precoder design with imperfect channel and battery knowledge," *IEEE Trans. Wireless Commun.*, vol. 13, no. 6, pp. 3137–3152, Jun. 2014.

[25] Z. Hu, T. Zhang, and J. Loo, "Power allocation for coordinated multi-cell systems with imperfect channel and battery-capacity-limited receivers," *IEEE Commun. Lett.*, vol. 21, no. 12, pp. 2746–2749, Dec. 2017.

[26] Z. Yang, Q. Han, B. Yang, B. Hu, C. Chen, and X. Guan, "Sum rate maximizing for SWIPT with limited battery capacity," in *Proc. 31st Youth Academic Annu. Conf. Chin. Assoc. Autom. (YAC)*, Nov. 2016, pp. 25–30.

[27] S. Mao, S. Leng, J. Hu, and K. Yang, "Utility-optimal resource allocation in energy harvesting powered C-RAN," in *Proc. IEEE Int. Conf. Commun. (ICC)*, May 2018, pp. 1–6.

[28] Z. Hu, C. Zheng, M. He, and H. Wang, "Joint Tx power allocation and Rx power splitting for SWIPT systems with battery status information," *IEEE Wireless Commun. Lett.*, vol. 9, no. 9, pp. 1442–1446, Sep. 2020.

[29] J. Ren, X. Lei, P. D. Diamantoulakis, Q. Chen, and G. K. Karagiannidis, "Buffer-aided secure relay networks with SWIPT," *IEEE Trans. Veh. Technol.*, vol. 69, no. 6, pp. 6485–6499, Jun. 2020.

[30] H. Mirghasemi, L. Vandendorpe, and M. Ashraf, "Optimal online resource allocation for SWIPT-based mobile edge computing systems," in *Proc. IEEE Wireless Commun. Netw. Conf. (WCNC)*, May 2020, pp. 1–8.

[31] S. Mao, S. Leng, S. Maharjan, and Y. Zhang, "Energy efficiency and delay tradeoff for wireless powered mobile-edge computing systems with multi-access schemes," *IEEE Trans. Wireless Commun.*, vol. 19, no. 3, pp. 1855–1867, Mar. 2020.

[32] H.-S. Lee and J.-W. Lee, "Resource and task scheduling for SWIPT IoT systems with renewable energy sources," *IEEE Internet Things J.*, vol. 6, no. 2, pp. 2729–2748, Apr. 2019.

[33] E. Boshkovska, D. W. K. Ng, N. Zlatanov, and R. Schober, "Practical non-linear energy harvesting model and resource allocation for SWIPT systems," *IEEE Commun. Lett.*, vol. 19, no. 12, pp. 2082–2085, Dec. 2015.

[34] Y. Zeng, B. Clerckx, and R. Zhang, "Communications and signals design for wireless power transmission," *IEEE Trans. Commun.*, vol. 65, no. 5, pp. 2264–2290, May 2017.

[35] M. J. Neely, "Stochastic network optimization with application to communication and queueing systems," *Synth. Lect. Commun. Netw.*, vol. 3, no. 1, pp. 1–211, 2010.

[36] D. Gross, J. F. Shortle, J. M. Thompson, and C. M. Harris, *Fundamentals of Queueing Theory*. Hoboken, NJ, USA: Wiley, 2008.

[37] D. Kumar, S. K. Joshi, and A. Tolli, "Latency-aware reliable mmWave communication via multi-point connectivity," in *Proc. IEEE Global Commun. Conf. (GLOBECOM)*, Dec. 2020, pp. 1–6.

[38] S. Boyd and L. Vandenberghe, *Convex Optimization*. Cambridge, U.K.: Cambridge Univ. Press, 2004.

[39] K. Shen and W. Yu, "Fractional programming for communication systems—Part I: Power control and beamforming," *IEEE Trans. Signal Process.*, vol. 66, no. 10, pp. 2616–2630, May 2018.

[40] A. Beck, A. Ben-Tal, and L. Tetruashvili, "A sequential parametric convex approximation method with applications to nonconvex truss topology design problems," *J. Global Optim.*, vol. 47, no. 1, pp. 29–51, Jul. 2010.

[41] Z.-Q. Luo, W.-K. Ma, A. So, Y. Ye, and S. Zhang, "Semidefinite relaxation of quadratic optimization problems," *IEEE Signal Process. Mag.*, vol. 27, no. 3, pp. 20–34, May 2010.

[42] H. Pennanen, A. Tölli, and M. Latva-Aho, "Decentralized robust beamforming for coordinated multi-cell MISO networks," *IEEE Signal Process. Lett.*, vol. 21, no. 3, pp. 334–338, Mar. 2014.

[43] M. Grant and S. Boyd. (Mar. 2014). *CVX: MATLAB Software for Disciplined Convex Programming*. [Online]. Available: http://cvxr.com/cvx

[44] E. Chen and M. Tao, "ADMM-based fast algorithm for multi-group multicast beamforming in large-scale wireless systems," *IEEE Trans. Commun.*, vol. 65, no. 6, pp. 2685–2698, Jun. 2017.

[45] N. D. Sidiropoulos, T. N. Davidson, and Z.-Q. Luo, "Transmit beamforming for physical-layer multicasting," *IEEE Trans. Signal Process.*, vol. 54, no. 6, pp. 2239–2251, Jun. 2006.

[46] D. Coppersmith and S. Winograd, "Matrix multiplication via arithmetic progressions," *J. Symbolic Comput.*, vol. 9, no. 3, pp. 251–280, 1990.

Onel L. Alcaraz López (Member, IEEE) was born in Sancti-Spíritus, Cuba, in 1989. He received the B.Sc. degree (Hons.) from the Central University of Las Villas, Cuba, in 2013, the M.Sc. degree from the Federal University of Paraná, Brazil, in 2017, and the D.Sc. degree (Hons.) from the University of Oulu, Finland, in 2020, all in Electrical Engineering. From 2013 to 2015, he was a Specialist of telematics at Cuban Telecommunications Company (ETECSA). He is currently an Assistant Professor (tenure track) of sustainable wireless communications engineering at the Centre for Wireless Communications (CWC), Oulu, Finland. He authored the book titled *Wireless RF Energy Transfer in the Massive IoT Era: Towards Sustainable Zero-Energy Networks* (Wiley, December 2021). His research interests include the sustainable IoT, energy harvesting, wireless RF energy transfer, wireless connectivity, machine-type communications, and cellular-enabled positioning systems. He is a Collaborator to the 2016 Research Award given by the Cuban Academy of Sciences, a co-recipient of the 2019 IEEE European Conference on Networks and Communications (EuCNC) Best Student Paper Award, the recipient of both the 2020 Best Doctoral Thesis Award granted by Academic Engineers and Architects in Finland TEK and Tekniska Föreningen i Finland TFiF in 2021 and the 2022 Young Researcher Award in the field of technology in Finland.

Satya Krishna Joshi (Member, IEEE) received the M.Eng. degree in telecommunications from the Asian Institute of Technology, Pathumthani, Thailand, in 2007, and the Ph.D. degree from the University of Oulu, Finland in 2018. His research interests include application of optimization techniques for signal processing and MIMO communications.

Antti Tölli (Senior Member, IEEE) received the Dr.Sc. (Tech.) degree in electrical engineering from the University of Oulu, Oulu, Finland, in 2008. From 1998 to 2003, he worked at Nokia Networks as a Research Engineer and a Project Manager both in Finland and Spain. In May 2014, he was granted a five year Academy Research Fellow post by the Academy of Finland, from 2014 to 2019. From 2015 to 2016, he visited at EURECOM, Sophia Antipolis, France, while from August 2018 to June 2019, he was at the University of California Santa Barbara, USA. He is a Professor with the Centre for Wireless Communications (CWC), University of Oulu. He has authored numerous papers in peer-reviewed international journals and conferences and several patents all in the area of signal processing and wireless communications. His research interests include radio resource management and transceiver design for broadband wireless communications with a special emphasis on distributed interference management in heterogeneous wireless networks. From 2017 to 2021 he served as an Associate Editor for IEEE TRANSACTIONS ON SIGNAL PROCESSING.

Dileep Kumar (Graduate Student Member, IEEE) received the master's degree in communication engineering from the IIT Bombay, India, in 2015, and the Dr.Sc. (Tech.) degree in communications engineering from the University of Oulu, Finland, in 2022. From 2015 to 2017, he was a Research Engineer at NEC Corporation, Tokyo, Japan. In 2018, he joined the Centre for Wireless Communications (CWC), University of Oulu. His research interests include signal processing for wireless communication systems.